Non-photopic and photopic visual cycles differentially regulate immediate, early, and late phases of cone photoreceptor-mediated vision

Received for publication, October 8, 2019, and in revised form, March 30, 2020 Published, Papers in Press, April 1, 2020, DOI 10.1074/jbc.RA119.011374

Rebecca Ward[‡], Joanna J. Kaylor[§], Diego F. Cobice[¶], Dionissia A. Pepe[‖], Eoghan M. McGarrigle[‖], Susan E. Brockerhoff[**‡‡], James B. Hurley[**‡‡], Gabriel H. Travis[§ §§1], and Breandán N. Kennedy[‡2]

*From the [‡]UCD School of Biomolecular and Biomedical Science, UCD Conway Institute, University College Dublin, Dublin D04 V1W8, Ireland, the [§]Jules Stein Eye Institute, UCLA School of Medicine, Los Angeles, California 90095, the [¶]Mass Spectrometry Centre, School of Biomedical Sciences, Biomedical Sciences Research Institute, Ulster University, Coleraine BT52 1SA, Northern Ireland, the [‖]Centre for Synthesis and Chemical Biology, UCD School of Chemistry, University College Dublin, Dublin D04 V1W8, Ireland, the Departments of **Biochemistry and [‡‡]Ophthalmology, University of Washington, Seattle, Washington 98109, and the [§§]Department of Biological Chemistry, UCLA School of Medicine, Los Angeles, California 90095*

Edited by Henrik G. Dohlman

Cone photoreceptors in the retina enable vision over a wide range of light intensities. However, the processes enabling cone vision in bright light (*i.e.* photopic vision) are not adequately understood. Chromophore regeneration of cone photopigments may require the retinal pigment epithelium (RPE) and/or retinal Müller glia. In the RPE, isomerization of all-*trans*-retinyl esters to 11-*cis*-retinol is mediated by the retinoid isomerohydrolase Rpe65. A putative alternative retinoid isomerase, dihydroceramide desaturase-1 (DES1), is expressed in RPE and Müller cells. The retinol-isomerase activities of Rpe65 and Des1 are inhibited by emixustat and fenretinide, respectively. Here, we tested the effects of these visual cycle inhibitors on immediate, early, and late phases of cone photopic vision. In zebrafish larvae raised under cyclic light conditions, fenretinide impaired late cone photopic vision, while the emixustat-treated zebrafish unexpectedly had normal vision. In contrast, emixustat-treated larvae raised under extensive dark-adaptation displayed significantly attenuated immediate photopic vision concomitant with significantly reduced 11-*cis*-retinaldehyde (11cRAL). Following 30 min of light, early photopic vision was recovered, despite 11cRAL levels remaining significantly reduced. Defects in immediate cone photopic vision were rescued in emixustat- or fenretinide-treated larvae following exogenous 9-*cis*-retinaldehyde supplementation. Genetic knockout of Des1 (*degs1*) or retinaldehyde-binding protein 1b (*rlbp1b*) did not eliminate photopic vision in zebrafish. Our findings define molecular and temporal requirements of the nonphotopic or photopic visual cycles for mediating vision in bright light.

Photopic vision is the physiological function mediating vision in well-lit conditions. Daytime vision requires cone photoreceptors to remain functional in the presence of light. This capability requires regeneration of cone photopigments in the retina prior to and during light onset. However, our understanding of the biological process contributing to immediate, early, and late phases of cone photopic vision is inadequate.

Sustained vision in vertebrates depends upon a supply of 11-*cis*-retinaldehyde (11cRAL)[3] chromophore to regenerate photobleached visual pigments. The canonical visual cycle is the enzymatic pathway in the retinal pigment epithelium (RPE) that recycles visual chromophore (1). The retinoid isomerase in RPE cells is RPE65, which converts all-*trans* retinyl esters (atREs), synthesized by lecithin–retinol acyltransferase, to 11-*cis*-retinol (11cROL) (2–4). Null mutations in the mouse *Rpe65* or *Lrat* gene cause the virtual absence of 11cRAL within the neural retina (5, 6). *Rpe65*$^{-/-}$ mice exhibit massive accumulation of atREs in the RPE, whereas retinoids are almost undetectable in the RPE of *Lrat*$^{-/-}$ mice (7, 8). Notably, there is still uncertainty as to if, and when, the RPE65 visual cycle contributes to cone photopic vision.

Under daylight conditions, the estimated rate of 11cRAL synthesis by RPE cells is much slower than the rate of chromophore consumption by rods and cones (9). Despite the non-contribution of rods to daylight vision, rhodopsin continues to photoisomerize in bright light exposed retinas. Cones must therefore compete with rods for chromophore when demand is

This work was supported by Irish Research Council/Fighting Blindness Grant EPSPG/2017/276 (to R. W.), European Union's Horizon 2020 Research and Innovation Staff Exchange Program under Grant 734907 (RISE/3D-NEONET Project) (to B. N. K.), National Institutes of Health NEI Grant R01-EY024379 (to G. H. T.), and National Institutes of Health Core Grant P30-EY000331. The authors declare that they have no conflicts of interest with the contents of this article. The content is solely the responsibility of the authors and does not necessarily represent the official views of the National Institutes of Health.

This article contains Fig. S1 and Table S1.

[1] The Charles Kenneth Feldman Professor of Ophthalmology at UCLA.

[2] To whom correspondence should be addressed: UCD School of Biomolecular and Biomedical Science, UCD Conway Institute, University College Dublin, Belfield, Dublin D04 V1W8, Ireland. E-mail: brendan.kennedy@ucd.ie.

[3] The abbreviations used are: 11cRAL, 11-*cis*-retinal; 11cROL, 11-*cis*-retinol; atROL, all-*trans*-retinol; atRAL, all-trans-retinal; atRP, all-trans-retinyl palmitate; CRISPR/Cas9, Clustered regularly interspaced short palindromic repeats/CRISPR-associated protein 9; DES1, dihydroceramide desaturase-1; MFAT, multifunctional *O*-acyltransferase; OKR, optokinetic response; RBP4, retinol-binding protein 4; RPE, retinal pigment epithelium; RBP4, retinol-binding protein 4; ZT, Zeitgeber; 9cRAL, 9-*cis*-retinal; 11cRE, 11-*cis*-retinyl ester; 11cRP, 11-*cis*-retinyl palmitate; ANOVA, analysis of variance; dpf, days post-fertilization; hpf, hours post-fertilization; ERG, electroretinography; RGR, retinal G protein–coupled receptor; PAM, protospacer adjacent motif; qRT-PCR, quantitative RT-PCR.

the highest. As a possible adaptation, cones can regenerate cone opsin pigments by uptake of either 11cRAL or 11cROL, although rods can only uptake 11cRAL (10–12). Müller glial cells of the neural retina are the likely source of this 11cROL (13). Dihydroceramide desaturase (DES1; encoded by *DEGS1*) and multifunctional *O*-acyltransferase (MFAT) represent another retinol isomerase—retinyl-ester synthase pair, present in Müller cells, which may mediate 11cROL synthesis. The "*isomerosynthase*" activity of DES1—MFAT is present in retinas from cone-dominant chickens and ground squirrels but is undetectable in retinas from rod-dominant mice and cattle (9, 14). This activity correlated with the presence of 11-*cis*-retinyl esters (11cREs) in the neural retina, which are undetectable in mice and cattle retinas. Interestingly, synthesis of 11cROL by DES1 is increased through interactions with cellular retinaldehyde–binding protein (CRALBP; encoded by *RLBP1*), an 11cRAL/11cROL carrier protein expressed in the RPE and Müller glia (15).

In contrast to the evidence supporting a role for DES1 in cone chromophore regeneration, a recent study reported that recovery of cone electrophysiological sensitivity, in isolated retinas following a photobleach, was similar in $Des1^{+/+}$ and Müller cell conditional $Des1^{-/-}$ mutant mice (16). This suggests Müller DES1 plays no role in the generation of retinoids to recover mouse cone electroretinograms. However, uncertainty remains regarding the overall contribution of DES1 to the cone visual cycle as significant DES1 activity remained in retinal lysates of these Müller cell $Des1^{-/-}$ mice. Additionally, the cone electrophysiological studies were conducted in rod-dominant mice, whereas DES1 was identified in Müller cells from cone-dominant chicken. Thus, uncertainly remains whether species specific retinoid isomerase pathways exist to meet cone chromophore demands.

Another mechanism postulated to replenish cones with chromophore is the photopic visual cycle, a process that regenerates 11cRAL by a light-dependent mechanism. The nonvisual opsin, retinal G-protein–coupled receptor (RGR) opsin, is present in RPE and Müller cells. Previous reports show RGR-opsin is integral to light-dependent biochemical formation of 11cRAL that reconstitutes rhodopsin visual pigment in rods (17). RGR-opsin appears essential for the recovery of cone electrophysiological sensitivity as retinas from WT mice under sustained background illumination maintained cone sensitivity, whereas $Rgr^{-/-}$ mice exhibited diminishing cone sensitivity during light exposure (18). Notably, all these studies assess cone electroretinography (ERG) and not cone vision. It is well-recognized that electrophysiology does not absolutely correlate to functional vision. For example, patients receiving gene therapy for RPE65 defects show no improvement in ERG but show significant improved ability to navigate an obstacle course (19).

Most visual cycle knowledge was ascertained by studying the retinae of rod-dominant mice. Consequently, investigations of the visual cycles enabling cone vision are less advanced. Zebrafish larvae provide novel opportunities to study cone photopic vision and the supporting visual cycle processes (20) due to easy genetic and pharmacological manipulation and cone-dominant vision until 15 dpf, the stage when rods become functional (21, 22). Previous studies investigating visual cycle components in zebrafish relied on transient morpholino knockdown. Zebrafish *rpe65a* knockdown significantly reduced but did not completely attenuate 11cRAL synthesis, supporting the presence of an alternative pathway for chromophore synthesis in zebrafish retinae (20). Knockdown of either Cralbpa or Cralbpb in zebrafish resulted in reduced visual behavior (23) and reduced light sensitivity (24).

Pharmacological modulators that inhibit or complement the visual cycles are potential treatments for retinal disease (25, 26). Following photoisomerization, released atRAL must be delivered to RPE/Müller cells to regenerate 11cRAL to restore light sensitivity. Impaired atRAL clearance from photoreceptors leads to accumulation of bis-retinoid *N*-retinylidene–*N*-retinylethanolamine, a toxic by-product of atRAL and a pathological hallmark of age-related macular degeneration and Stargardt's disease (27). Emixustat (ACU-4429) competitively inhibits Rpe65 and hinders retinaldehyde-mediated destruction of photoreceptors by acting as a retinaldehyde scavenger (26). Inhibition of chromophore synthesis gives rise to unliganded "noisy" opsins that stimulate the transduction pathway in the absence of light, greatly decreasing photoreceptor sensitivity (28). In $Rpe65^{-/-}$ mice, chronic activation of signal transduction may cause photoreceptor degeneration (29). Free opsin can be targeted by chromophore replacement therapy with 9cRAL, which bypasses the visual cycle defect to form isorhodopsin or iso-cone opsins. Following 9cRAL treatment, light sensitivity is restored long-term in $Rpe65^{-/-}$ mice with attenuated accumulation of atREs (30). Fenretinide, a derivative of retinoic acid, is reported to inhibit DES1 without affecting RPE65 activity (31–33). Fenretinide also competes with retinol for binding to retinol-binding protein (RBP4) in blood, causing a mild vitamin A deficiency (34). A1120 is a nonretinoid RBP4 antagonist, which in mice reduces serum retinol levels in a dose-dependent manner (35) and reduces lipofuscin accumulation in $Abca4^{-/-}$ mice through reduction of serum RBP4 and visual retinoids (34). Unlike fenretinide, A1120 does not act as a retinoic acid receptor α agonist. A1120 does not affect RPE65 isomerohydrolase activity in *ex vivo* experiments (34).

Previous visual cycle inhibition studies focused on measuring retinal function (*e.g.* electrophysiology) as the primary end point. Reduced cone photosensitivity was observed in live mice, *ex vivo* mouse retinae, and in ground squirrels treated with visual cycle inhibitors (32). To our knowledge, no previous studies investigated the relationship between visual cycle modulation and cone photopic visual behavior. In this study, we used visual behavior assays, visual cycle inhibitors, and genetic approaches in zebrafish to understand the mechanisms regulating immediate (at light onset following dark adaptation, 0 min), early (after 30 min light adaptation), or late (after ~4–6 h light adaptation) phases of cone photopic vision. Original findings were uncovered in relation to cone photopic vision, including: (i) late photopic vision is significantly impaired by fenretinide, but not by emixustat; (ii) immediate photopic vision is reliant on Rpe65; (iii) 30 min of light is sufficient to restore early photopic vision and surmount the RPE65 inhibitor emixustat; (iv) the RPE65-independent recovery of early photopic vision occurs with low levels of 11cRAL; (v) exogenous 9cRAL is sufficient to restore photopic vision; and (vi) photopic vision was not eliminated upon knockout of *degs1* or RPE-expressed *rlbp1b*.

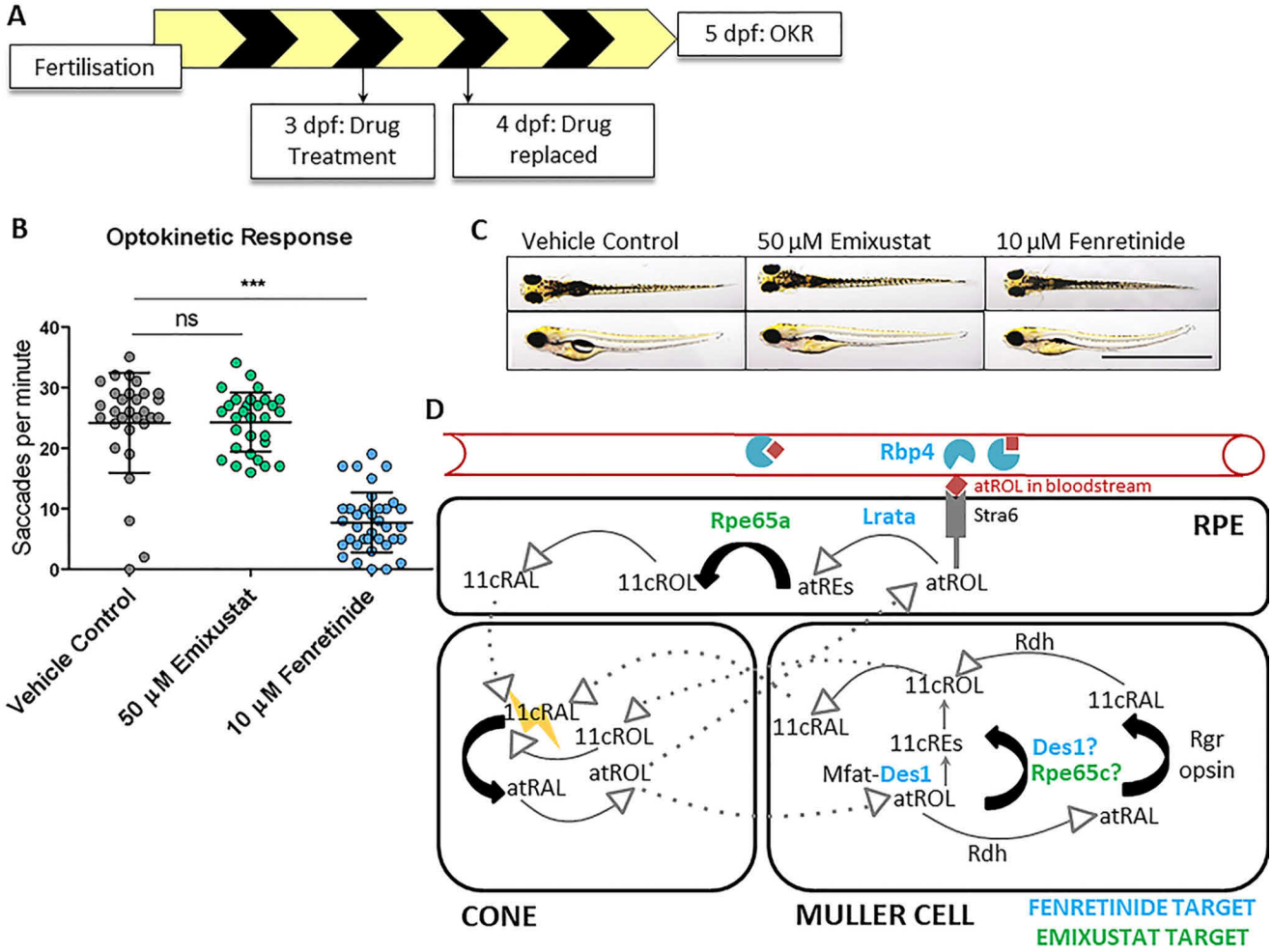

Figure 1. Fenretinide, but not emixustat, impairs late cone photopic vision in zebrafish larvae. *A,* schematic representation of experimental workflow. Zebrafish larvae were treated initially at 3 dpf, and the drug was replaced at 4 dpf. Larvae were incubated under standard lighting conditions (14 h light and 10 h dark) until OKR analysis at 5 dpf. *B,* OKR in 5 dpf larvae following treatment with 50 μM emixustat and 10 μM fenretinide. Data were analyzed by one-way ANOVA and Dunnett's multiple comparisons post hoc test, where *ns* = not significant ($p > 0.05$) and *** = $p < 0.001$. $n = 30$ larvae with three independent biological replicates. *C,* dorsal and lateral bright-field microscopy images of larvae following treatment with 50 μM emixustat or 10 μM fenretinide at 5 dpf. *Scale bar* = 2 mm. *D,* schematic overview mapping all possible mechanisms of cone chromophore regeneration in zebrafish, including the confirmed molecular targets of both emixustat and fenretinide. Proteins colored in *blue* depict fenretinide targets (Rbp4, Lrata, and Des1), and those in *green* highlight (potential) targets of emixustat (Rpe65a and Rpe65c) in zebrafish.

Results

Fenretinide, but not emixustat, impairs late cone photopic vision in zebrafish larvae

To investigate the effects of visual cycle inhibitors on cone vision, we assayed the effects of pharmacological agents, previously used in human clinical trials (36, 37), on the vision of 5 dpf zebrafish larvae. Previous studies demonstrate 5 dpf zebrafish rely exclusively on cones for vision (38). Emixustat is a potent RPE65 inhibitor, whereas targets of fenretinide include DES1 (the putative isomerase II) (32) and retinol-binding protein 4 (Rbp4) in blood (34). Larvae were raised under normal cyclic light conditions (14 h light and 10 h dark) for the duration of the experiment and treated with emixustat or fenretinide from 3 dpf. Drug was replenished at 4 dpf, and OKR analysis was completed at 5 dpf between ZT 2.5 and ZT 6.5 (Fig. 1*A*). OKR parameters used for all experiments were 20 alternating black and white stripes (18° per stripe, 99% contrast) rotated at 18 rpm. Surprisingly, late photopic vision was unaffected in 5 dpf larvae treated with up to 50 μM emixustat (24.3 ± 4.9 saccades per min) (Fig. 1*B*). In contrast, larvae treated with 10 μM fenretinide displayed significantly fewer ($p < 0.001$) saccades per min (7.7 ± 5), compared with vehicle controls (24.2 ± 8.2) (Fig. 1*B*). Whole-mount images reveal that 5 dpf larvae treated with emixustat or fenretinide fail to inflate their swim bladder, but otherwise have normal gross morphology (Fig. 1*C*). Fig. 1*D* depicts potential targets of emixustat and fenretinide in zebrafish. Zebrafish have three *rpe65* isoforms, two of which are expressed in the eye (20, 39). Emixustat may inhibit RPE-expressed *rpe65a* or Müller-cell expressed *rpe65c* (Fig. 1*D*). Fenretinide may inhibit Des1 isomerase activity in Müller cells/RPE or inhibit uptake of atROL from the serum by blocking Rbp4–transthyretin interactions. In summary, in cyclic lighting conditions, a broad-spectrum visual cycle inhibitor impairs late photopic vision, whereas a selective inhibitor of the canonical visual cycle did not affect vision.

In dark-adapted zebrafish, emixustat blocks immediate photopic vision and fenretinide exerts an additive effect

As Rpe65 is important for chromophore regeneration under dark conditions, we tested the visual cycle inhibitors in dark-

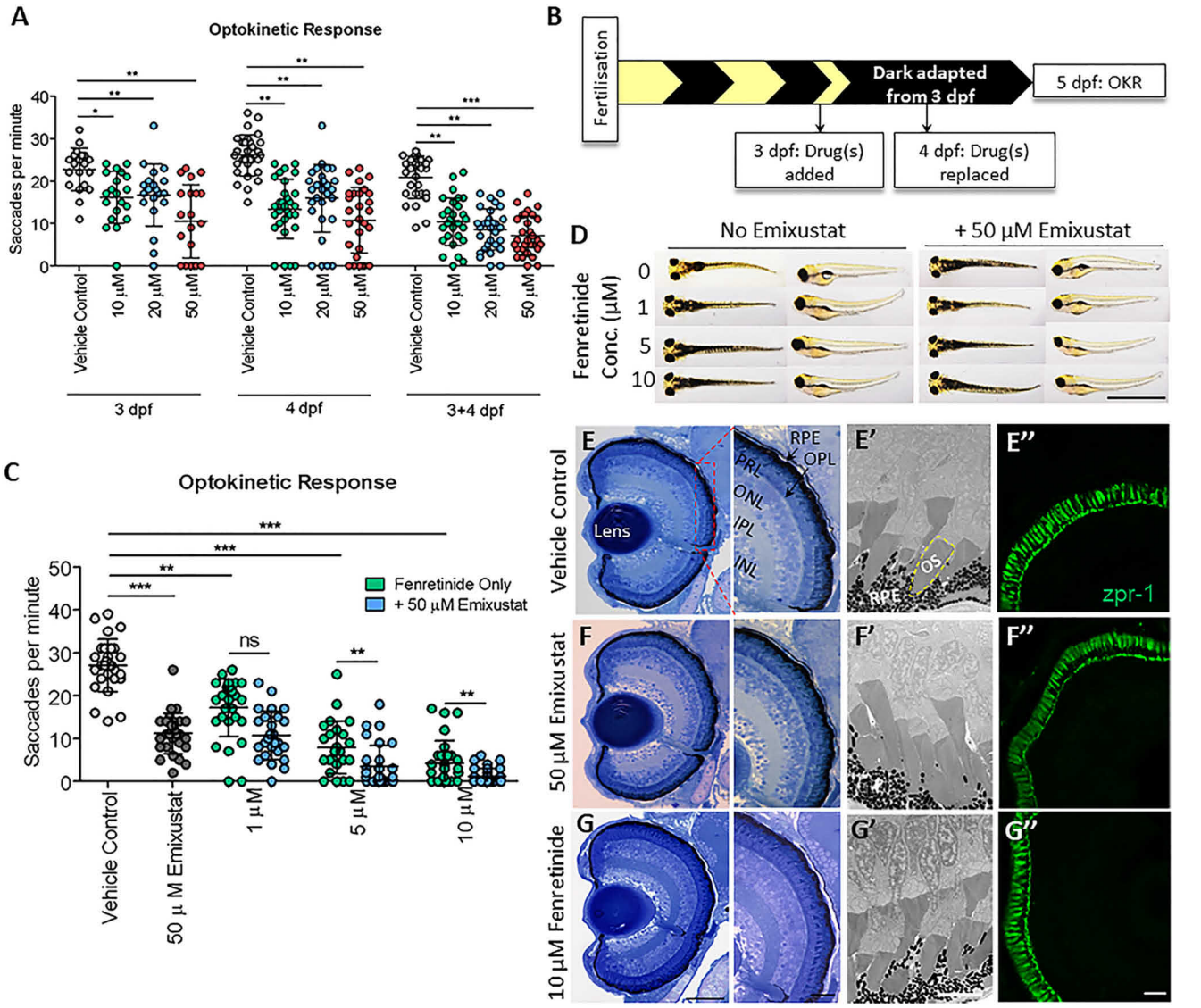

Figure 2. In dark-adapted zebrafish, emixustat blocks immediate photopic vision and fenretinide exerts an additive effect. *A,* optimization of dose and treatment time points for emixustat. Larval OKR at 5 dpf following treatment with 10, 20, or 50 μM emixustat at 3, 4, and 3 and 4 dpf. Data were analyzed by two-way ANOVA and Bonferroni post hoc test, where * = $p < 0.05$, ** = $p < 0.01$, and *** = $p < 0.001$. $n = 30$ larvae with three independent biological replicates. *B,* schematic representation of experimental workflow. Zebrafish larvae were initially treated with emixustat and/or fenretinide at 3 dpf, and drug(s) were replaced at 4 dpf. Larvae were incubated under dark conditions until OKR analysis at 5 dpf. *C,* larval OKR at 5 dpf following combination treatment with 50 μM emixustat and/or 10 μM fenretinide at days 3 and 4. Data were analyzed by two-way ANOVA and Bonferroni post hoc test, where *ns* = not significant and ** = $p < 0.01$. *D,* dorsal and lateral bright-field microscopy images of larvae at 5 dpf following treatment with 50 μM emixustat and/or 10 μM fenretinide. *Scale bar* = 2 mm. *E,* retinal morphology of 5 dpf larvae treated with 0.5% DMSO, 50 μM emixustat, or 10 μM fenretinide. Retinal bright-field images taken with a ×60 and ×100 objective. *PRL,* photoreceptor layer; *OPL,* outer plexiform layer; *ONL,* outer nuclear layer; *IPL,* inner plexiform layer; *INL,* inner nuclear layer. *Scale bar* = 50 and 20 μm, respectively. *E′–G′*, high-resolution images of photoreceptor outer segments (*OS, yellow dotted line*) and RPE in 5 dpf larvae. *Scale bar* = 5 μm. *E″–G″*, immunohistochemistry on transverse section across lens at 5 dpf. Double cones were stained with zpr-1 antibody. *Scale bar* = 20 μm.

adapted zebrafish larvae wherein larvae were raised under normal cyclic light conditions until 3– 4 dpf, then treated with drug under constant dark conditions until 5 dpf. Dose-response and dose-frequency studies revealed that 50 μM emixustat added at day 3 and replaced at day 4 caused the most significant reduction in OKR saccade numbers/min (7.1 ± 4.6, $p < 0.001$) compared with vehicle controls (20.9 ± 5) (Fig. 2*A*). Larvae were then treated with a combination of emixustat and fenretinide. Drug(s) were added at 3 dpf and replaced at 4 dpf, and visual behavior analysis was performed between ZT 2.5 and ZT 6.5 on 5 dpf, wherein the larvae were individually removed from wells and immediately subjected to OKR following a 2-day dark adaptation (Fig. 2*B*). Under dark conditions, larvae treated with 10 μM fenretinide displayed an ~6-fold reduction in the ability to track 1 cm thick rotating stripes, whereas larvae treated with 50 μM emixustat had an ~2.5-fold decrease in OKR. Interestingly, when both isomerase inhibitors were combined, immediate photopic vision was completely abolished (1.2 saccades/min, $p < 0.001$) and reduced by ~22-fold, compared with vehicle controls (26.8 saccades per min) (Fig. 2*C*). Larvae treated with emixustat and fenretinide in the dark were morphologically normal, other than they did not inflate their swim bladder (Fig. 2*D*) as also observed under a normal light/dark cycle (Fig. 1*C*). An uninflated swim bladder is commonly observed in visually-compromised zebrafish larvae (40, 41). Interestingly, neither 50 μM emixustat nor 10 μM fenretinide

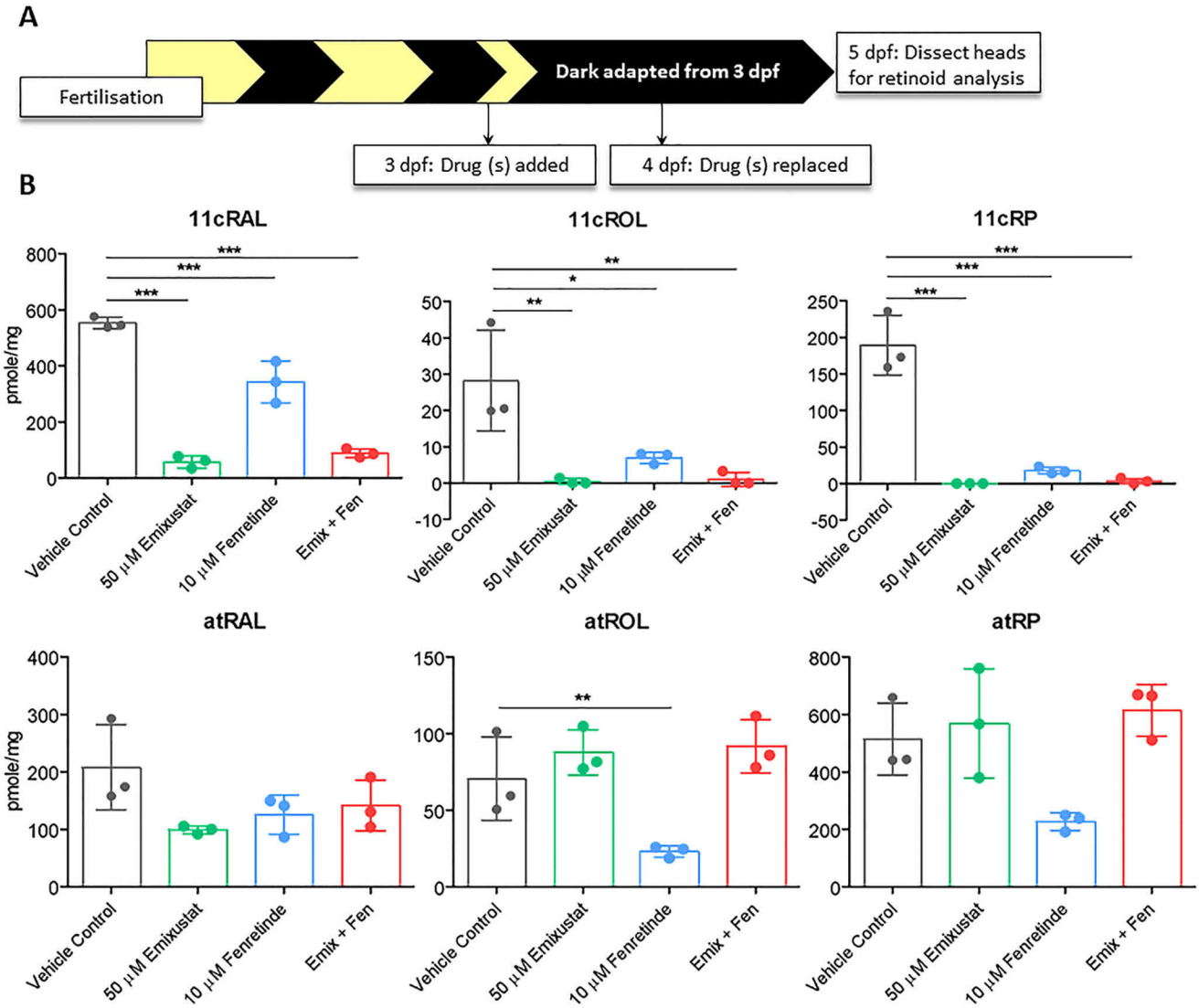

Figure 3. Visual cycle inhibitors modulate the profile of key retinoids in zebrafish. *A,* schematic representation of experimental workflow. Zebrafish larvae were initially treated with 50 μM emixustat and/or 10 μM fenretinide at 3 dpf, and the drug was replaced at 4 dpf. Larvae were incubated under dark conditions until the collection of larval heads for retinoid analysis at 5 dpf. *B,* retinoid profiles of 5 dpf larvae treated with emixustat and fenretinide, alone and in combination. *Bars* represent the mean ± S.D. of three independent experiments for each condition with 105 larval heads per biological replicate. Data were analyzed by a one-way ANOVA and Dunnett's multiple comparisons post hoc test, where * = $p < 0.05$, ** = $p < 0.01$, and *** = $p < 0.001$.

induced obvious changes in retinal histology, particularly the photoreceptor outer segment structure and RPE, compared with vehicle controls (Fig. 2, *E–G* and *E′–G′*). Furthermore, double cones stained with zpr-1 appear unaffected by fenretinide or emixustat treatment (Fig. 2, *E″–G″*). Thus, emixustat impaired immediate photopic vision following dark adaptation (Fig. 2, *A* and *C*) but not late photopic vision (Fig. 1*B*), whereas fenretinide inhibited both immediate and late photopic vision.

Visual cycle inhibitors modulate the profile of key retinoids in zebrafish

To assess the pharmacological specificity of the phenotypes in zebrafish, we measured the content of visual retinoids in zebrafish larval heads following pharmacological visual cycle inhibition. Animals genetically or pharmacologically devoid of functional visual cycles can present with significantly-altered levels of retinoids in the eye and liver (3, 20, 24, 26, 42, 43). In agreement with the impaired immediate photopic vision we observe in zebrafish, we observed a significant reduction in 11cRAL, 11cROL, and the 11cRE, 11-*cis*-retinyl palmitate (11cRP), following emixustat and fenretinide treatment, alone or in combination ($p < 0.001$) (Fig. 3*B*). Rpe65 uses atREs as its substrate; therefore, elevated levels could be expected in the presence of emixustat (2). Interestingly, atROL (23.2 ± 3.8 pmol/mg, $p < 0.01$) was significantly reduced in fenretinide-only treated larvae compared with the vehicle control (70.5 ± 27.3). These data suggest that emixustat and fenretinide impair immediate photopic vision following dark adaptation in zebrafish by reducing 11cRAL levels.

Supplementation with exogenous 9cRAL significantly improves immediate photopic vision in emixustat- and fenretinide-treated larvae

As cone function is partially restored in *Rpe65*$^{-/-}$ mice following treatment with 9cRAL, a functional analogue of 11cRAL

(44), we measured cone vision following treatment with exogenous 9cRAL. Larvae were treated with emixustat and/or fenretinide under dark-adapted conditions as described above (Fig. 2*B*). In addition, larvae were treated with 9cRAL 4 h following treatment with emixustat and/or fenretinide at both 3 and 4 dpf (Fig. 4*A*). Immediate photopic vision in emixustat-treated larvae supplemented with 9cRAL improved significantly (16.1 ± 6.7 saccades per min, $p < 0.001$), compared with emixustat treatment alone (10.5 ± 4.8 saccades per min) (Fig. 4*B*). We also observed ~2-fold (6.5 ± 5.5 saccades per min, $p < 0.01$) improved cone vision in fenretinide-treated larvae following supplementation with 9cRAL (Fig. 4*B*). Addition of exogenous 9cRAL also improved vision in emixustat- plus fenretinide-treated larvae ~5-fold compared with emixustat- and fenretinide-treated larvae without 9cRAL supplementation (5.3 *versus* 4.2 saccades per min, respectively) (Fig. 4*B*). No gross morphological changes were observed in larvae treated with 9cRAL in combination with either drug alone or in addition to fenretinide plus emixustat (Fig. 4*C*). Interestingly, larvae treated with emixustat and 9cRAL inflated their swim bladders (Fig. 4*C*), a characteristic not observed in larvae treated with emixustat alone (Fig. 2*D*). Finally, treatment of larvae with exogenous 9cRAL altered retinoid profiles at 5 dpf (Fig. 4*D* and Fig. S1). All 9-*cis*-retinoids (9cRP, 9cROL, and 9cRAL) and atRP significantly increased in emixustat plus 9cRAL-treated larvae, compared with emixustat alone. Interestingly, no significant increase was observed in 11cRAL profile following 9cRAL supplementation. Thus, the reduction in immediate photopic vision in emixustat- and fenretinide-treated larvae results not from toxic effects but rather from visual cycle inhibition.

Early photopic vision recovers in emixustat-treated larvae following exposure to light

Recent studies proposed the noncanonical visual cycle depends on an Rpe65-independent isomerization event that relies on RGR-opsin and occurs during sustained exposure to visible light (18). We hypothesized that exposure of larvae to light for 30 min following a prolonged dark adaptation may activate the alternative pathway and modulate the impaired visual behavior in larvae treated with emixustat and fenretinide under dark-adapted conditions (Fig. 2*C*). At 5 dpf, between ZT 2.5 and ZT 6.5, larvae were subjected to our standard OKR assay immediately after dark adaptation for 2 days (0 min) or following 30 min of subsequent exposure to ambient light (Fig. 5*A*). Pre-treatment with 50 μM emixustat partially suppressed immediate photopic vision in dark-adapted larvae (11.4 ± 7.6 saccades per min, $p < 0.001$) compared with vehicle controls (17.3 saccades per min) (Fig. 5*B*). In contrast, pre-treatment with 10 μM fenretinide virtually abolished immediate cone photopic vision in dark-adapted larvae (1.7 ± 3 saccades per min, $p < 0.0.001$) compared with the vehicle control (17.3 ± 4.5 saccades per min) (Fig. 5*B*). To help discriminate whether fenretinide acts via Rbp4 or Des1, A1120, a potent Rbp4 inhibitor, was tested. Similar to fenretinide, A1120 suppressed immediate cone photopic vision (10.2 ± 6.6 saccades per min). Subsequent exposure of untreated larvae to 30 min of light had a minimum effect on early cone visual function *versus* untreated, dark-adapted larvae (Fig. 5*B*).

Interestingly, early photopic vision in emixustat-treated larvae was indistinguishable from vehicle-only treated larvae after a 30-min exposure to light (Fig. 5*B*), despite lower 11cRAL levels in larvae treated with emixustat (Fig. 5*C*). Pre-treatment of larvae with fenretinide virtually abolished cone vision following 30 min of light exposure, similar to fenretinide-treated, dark-adapted larvae (Fig. 5*B*). Surprisingly, early photopic vision in A1120-treated larvae recovered to vehicle control levels (21 ± 5 saccades per min) indicating that the block in early photopic vision observed following fenretinide treatment is not a result of inhibiting Rbp4 (Fig. 5*B*).

The relatively normal cone OKRs in emixustat-treated larvae following light exposure raised the question whether this correlated with increased 11cRAL chromophore levels. Retinoid levels were profiled in emixustat-treated larval heads at 0 and 30 min of light exposure (Fig. 5*C*). Although vision recovered following 30 min of light exposure (Fig. 5*B*), 11cRAL levels surprisingly did not change. Interestingly, atRAL levels returned to that of the vehicle control following 30 min of light indicating photoisomerization of light-sensitive chromophore and activation of the phototransduction cascade.

As early photopic vision, in the presence of emixustat, recovered following exposure to ambient light for 30 min, there was a possibility of light-induced degradation or inactivation of emixustat. To test this possibility, we performed MS analysis of emixustat before and after light exposure. No change in the relative abundance of the ion corresponding to emixustat (m/z = 263.81—264.26) was observed (Fig. 5*D*). NMR analysis also demonstrated no chemical change to emixustat upon exposure to visible light (Fig. 5*E*).

To confirm that early photopic vision was not mediated by reactivation of RPE65, larvae were treated in the dark with emixustat from 3 dpf, and emixustat was removed at 5 dpf under dim red light, 30 min before OKR analysis at ZT 2.5 to ZT 6.5. OKR was conducted at 0- and 30-min post light exposure (Fig. 6*A*). As before, emixustat-treated larvae presented with significantly reduced immediate photopic vision following dark adaptation (13.8 ± 6.1 saccades per min, $p = 0.0003$), which recovered 30 min post light exposure (23.4 ± 6.5, $p < 0.0001$) (Fig. 6*B*). Retinoid analysis revealed a reduction in 11cRAL, which did not recover following a 30-min absence of emixustat and/or 30 min of light exposure (Fig. 6*C*). A significant increase in atRP in emixustat-treated larvae in both the 0- and 30-min groups reaffirms Rpe65 inhibition (Fig. 6*C*). In summary, although emixustat-treated WT larvae display impaired immediate photopic vision, larvae can regain vision following 30 min of light exposure. This light-dependent recovery of early photopic vision is not due to Rpe65 isomerase activity.

Des1 knockout does not eliminate cone photopic vision in zebrafish at 5 dpf

Controversially, previous studies implicated DES1 as the isomerase II in regeneration of cone visual pigments through the intraretinal visual cycle (15). To test whether Des1 is an important modulator of cone photopic vision, we created *degs1*$^{-/-}$ zebrafish using CRISPR/Cas9 by engineering a 484-bp deletion in exon 2 (Fig. 7*A*). Expression of *degs1* was analyzed with primers that span the deletion (primer set 2) or

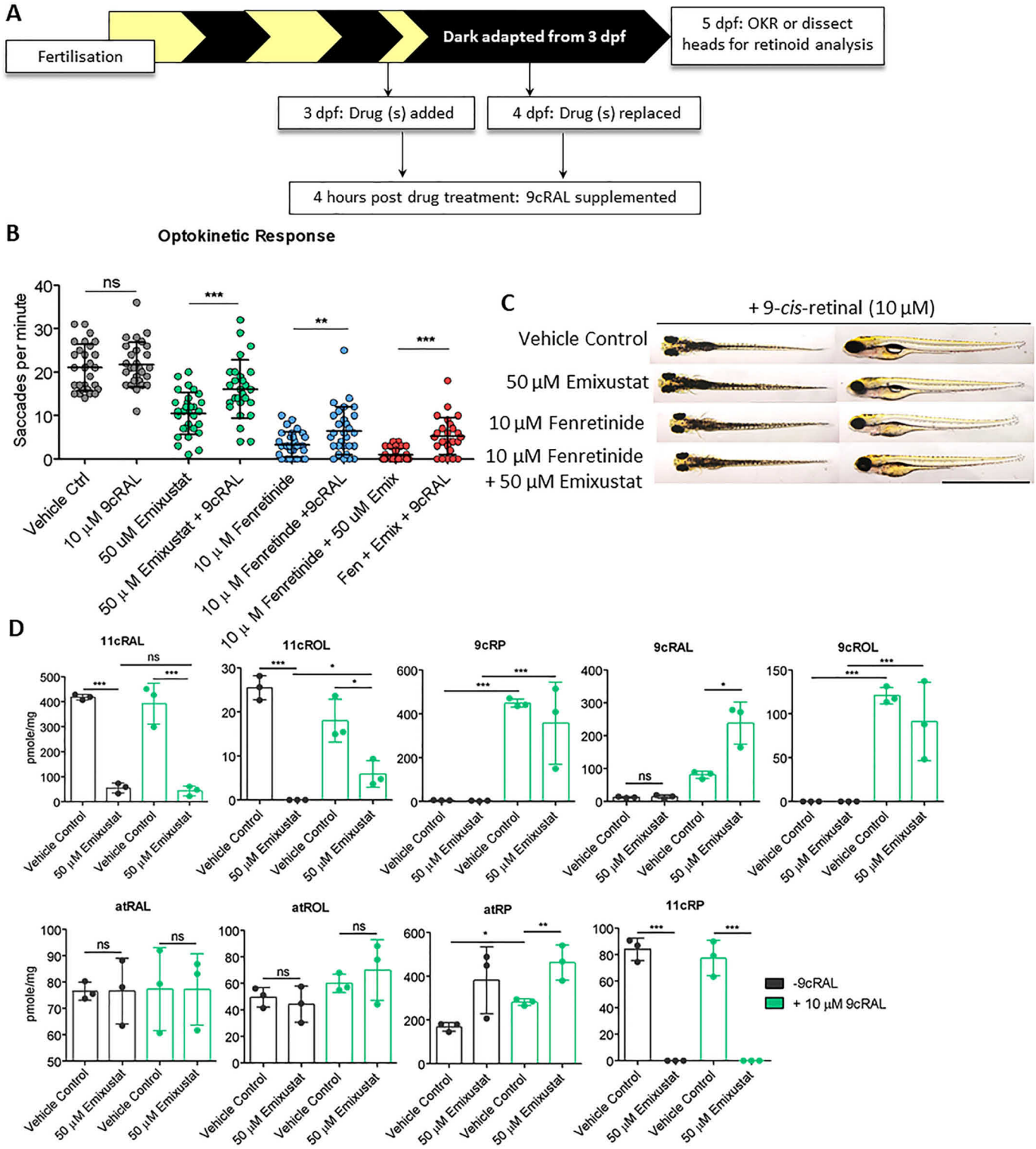

Figure 4. Supplementation with exogenous 9cRAL significantly improves immediate photopic vision in emixustat- and fenretinide-treated larvae. *A,* schematic representation of experimental workflow. Zebrafish larvae were treated initially at 3 dpf, and the drug was replaced at 4 dpf. 9cRAL was added to the medium 4 h following 50 μM emixustat and/or 10 μM fenretinide treatment on both 3 and 4 dpf. Larvae were incubated in the dark until OKR analysis at 5 dpf. *B,* larval OKR following addition of 10 μM 9cRAL to larvae previously treated with 50 μM emixustat and 10 μM fenretinide, alone or in combination at 3 and 4 dpf. Data were analyzed by unpaired, two-tailed *t* tests, where * = $p < 0.05$, ** = $p < 0.01$, and *** = $p < 0.001$. *ns* = not significant. $n = 30$ larvae with three independent biological replicates. *C,* dorsal and lateral bright-field microscopy images of larvae at 5 dpf larvae treated with 50 μM emixustat and/or 10 μM fenretinide in combination with 10 μM 9cRAL. *Scale bar* = 2 mm. *D,* retinoid profiles following exogenous 9cRAL supplementation in vehicle control and emixustat-treated zebrafish larvae. *Bars* represent the mean ± S.D. of three independent experiments for each condition with 105 larval heads per biological replicate. Data were analyzed by unpaired, two-tailed *t* tests, where * = $p < 0.05$, ** = $p < 0.01$, and *** = $p < 0.001$. *ns* = not significant.

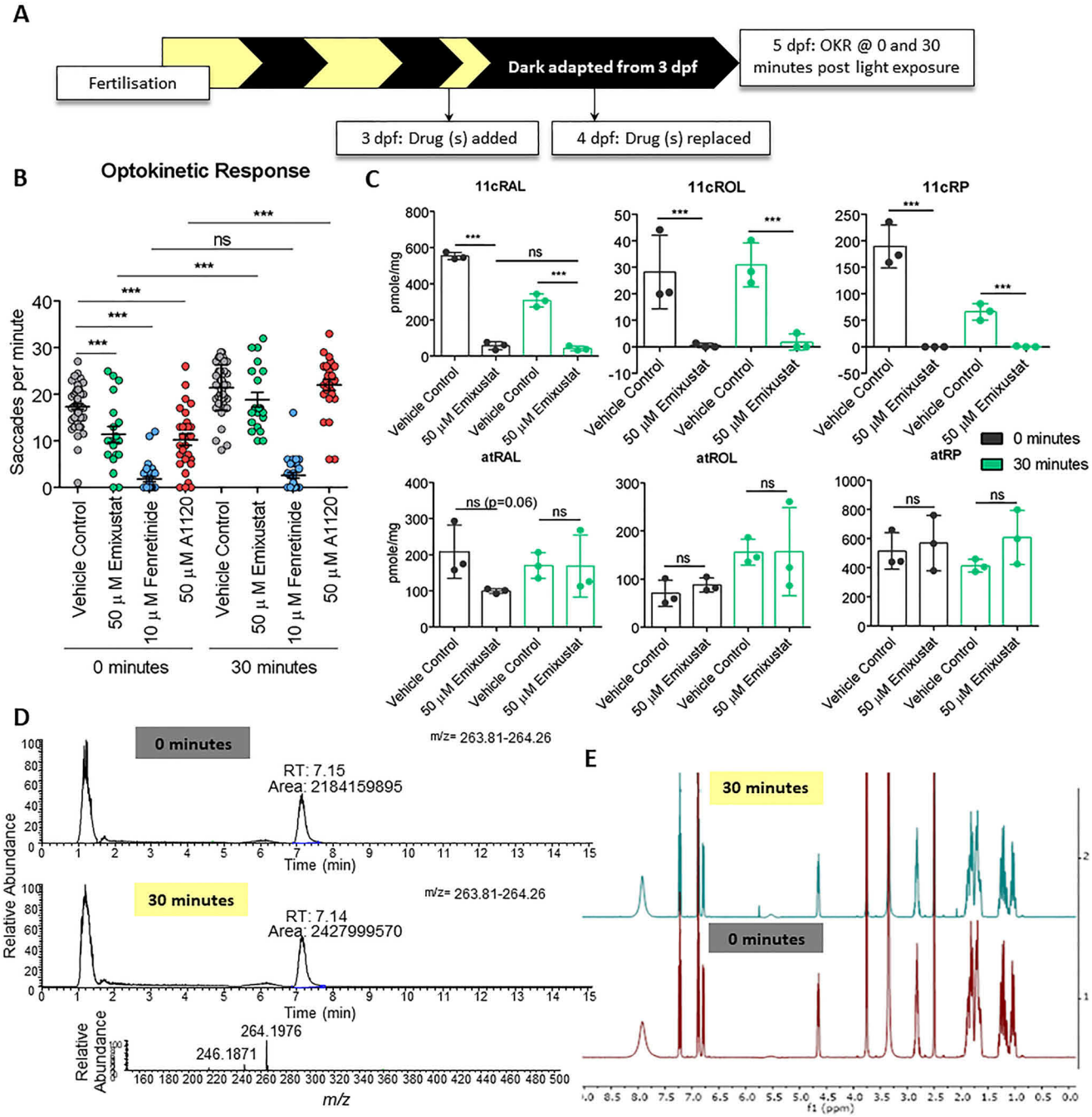

Figure 5. Early photopic vision recovers in emixustat-treated larvae following exposure to light. *A,* schematic representation of experimental workflow. Zebrafish larvae were treated initially at 3 dpf, and drug was replaced at 4 dpf. Larvae were incubated under dark conditions until analysis at 5 dpf. At 5 dpf, larvae were subjected to OKR immediately following dark adaptation (0 min) or following 30 min of light (30 min). *B,* OKR of 5 dpf larvae treated with 50 μM emixustat, 50 μM A1120, or 10 μM fenretinide 0 and 30 min following light exposure. Data were analyzed by unpaired, two-tailed *t* tests, where *ns* = not significant; *** = $p < 0.001$. $n = 30$ larvae with three independent biological replicates. *C,* retinoid profiles of 5 dpf larvae treated with 50 μM emixustat following no light exposure (0 min) or 30 min of light exposure (*30 min*). *Bars* represent the mean ± S.D. of three independent experiments for each condition with 105 larval heads per biological replicate. Data were analyzed by unpaired, two-tailed *t* tests, where *ns* = not significant and *** = $p < 0.001$. *D,* emixustat-extracted ion chromatograms (at *m/z* 264, RT 7.1 min) and high-resolution mass spectrum (*m/z* 264.1976 $[M + H]^+$) highlighting no change in the MS profile of emixustat exposed to 30 min of light and samples that received no light (0 min). *E,* NMR light sensitivity analysis of emixustat. Emixustat was dissolved in DMSO-d_6 (600 μl) covered with aluminum foil until ^{1}H NMR and HSQC experiments were performed (0 min). The NMR tube was left exposed to visible light for 30 min, followed by a second NMR analysis (30 min). Peaks at 2.09 and 5.76 ppm correspond to acetone and dichloromethane, respectively.

are nested within the deleted site (primer set 3) (Fig. 7*A*). Primer set 2 amplified a lower band of 61 bp indicating the presence of the transcript with deletion; however, it did not amplify the upper (537 bp) product observed in WT and *degs1*$^{+/-}$ samples (Fig. 7*B*). Moreover, when primer set 3 was used, a 162-bp product is seen in WT and *degs1*$^{+/-}$ lanes, although no product was amplified from *degs1*$^{-/-}$ samples (Fig. 7*B*). No gross morphological differences were observed in *degs1*$^{-/-}$ larvae at 5 dpf, compared with their unaffected siblings (Fig. 7*C*). Late photopic vision at ZT 2.5–6.5 is not signif-

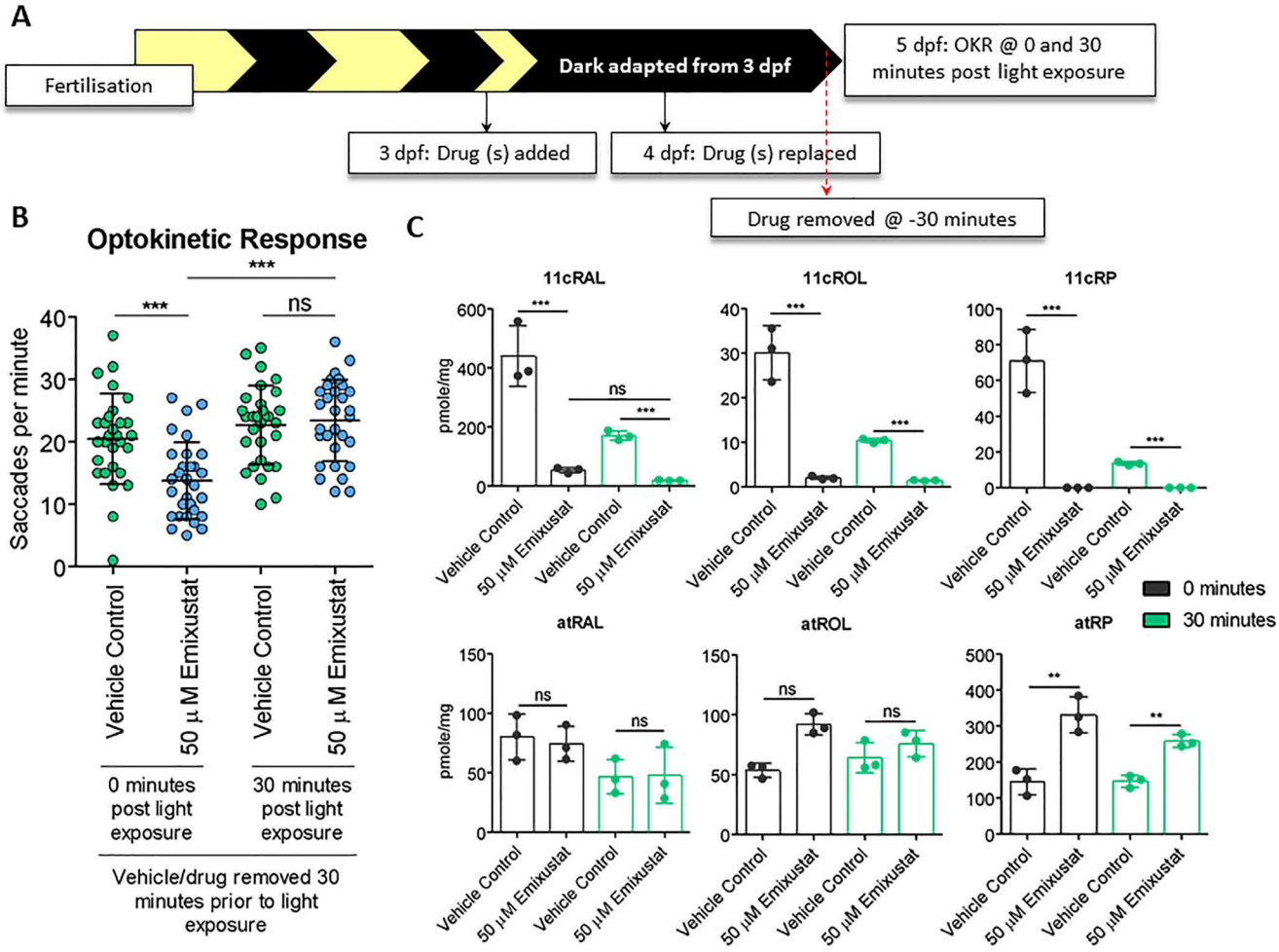

Figure 6. In the absence of light, 30 min alone is not sufficient to restore vision or 11cRAL levels. *A,* schematic representation of experimental workflow. Zebrafish larvae were treated initially at 3 dpf, and drug was replaced at 4 dpf. Larvae were incubated under dark conditions until analysis at 5 dpf. At 5 dpf, emixustat was removed under dim red light 30 min before larvae were subjected to OKR immediately following dark adaptation (0 min) or following 30 min light adaptation (30 min). *B,* optokinetic response 30 min following removal of emixustat at 5 dpf larvae 0 and 30 min following light exposure. Data were analyzed by unpaired, two-tailed *t* tests, where *ns* = not significant, ** = $p < 0.01$, and *** = $p < 0.001$. $n = 30$ larvae with three independent biological replicates. *C,* retinoid profiles of 5 dpf larvae treated with 50 μM emixustat. Emixustat was removed 30 min before dissection at 0- or 30-min post light exposure. *Bars* represent the mean ± S.D. of three independent experiments for each condition with 105 larval heads per biological replicate. Data were analyzed by unpaired, two-tailed *t*-tests, where *ns* = not significant; ** = $p < 0.01$, and *** = $p < 0.001$.

icantly affected in *degs1*$^{-/-}$ larvae (18.5 ± 5.4 saccades per min) at 5 dpf compared with unaffected *degs1*$^{+/+}$ or *degs1*$^{+/-}$ siblings (17.1 ± 5.3 saccades per min) (Fig. 7, *D* and *E*). We randomly drug-treated offspring from a *degs1*$^{+/-}$ in cross with 50 μM emixustat and incubated in the dark (Fig. 7*F*). Interestingly, neither immediate nor early photopic vision is significantly affected between the populations treated with vehicle or 50 μM emixustat (Fig. 7*G*). A genotyped sample of each group validated the normal photopic response of *degs1*$^{-/-}$ larvae (Fig. 7*H*).

Knockout of RPE-expressed rlbp1b does not eliminate cone photopic vision in zebrafish at 5 dpf

Co-immunoprecipitation experiments revealed that *RLBP1*-encoded CRALBP interacts with DES1 and increases the rate of 11cROL synthesis (15). Zebrafish *rlbp1* has subfunctionalized, with *rlbp1a* expressed in Müller cells and *rlbp1b* expressed in the RPE (25, 26). Here, a zebrafish knockout of RPE-expressed *rlbp1b* was created using CRISPR/Cas9, which introduced a 1440-bp deletion across exons 2 and 3 (Fig. 8*A*). Following *rlbp1b* knockout, *rlbp1b* gene expression was completely abolished ($p < 0.0001$) in *rlbp1b*$^{-/-}$ F_2 larval eyes (Fig. 8*C*). Gross morphology of *rlbp1b*$^{-/-}$ larvae is identical to their siblings at 5 dpf (Fig. 8*D*). Previous studies report a reduction in cone vision and function following *Rlbp1b* knockdown (25, 26); here, however, no differences in immediate ($p = 0.59$), early ($p = 0.9$), or late photopic vision ($p = 0.24$) were observed when tested under standard OKR conditions (Fig. 8, *E* and *F*).

Discussion

Many daily tasks are dependent on the ability of the eye to functionally adapt to changes in light. Vision in well-lit environments is known as photopic vision and is mediated by cone photoreceptors (45). Little is known regarding the biological processes underpinning functional photopic vision. Here, we apply chemical biology and genetics to dissect the contribution of light, retinoids, retinoid carrier proteins, and retinoid iso-

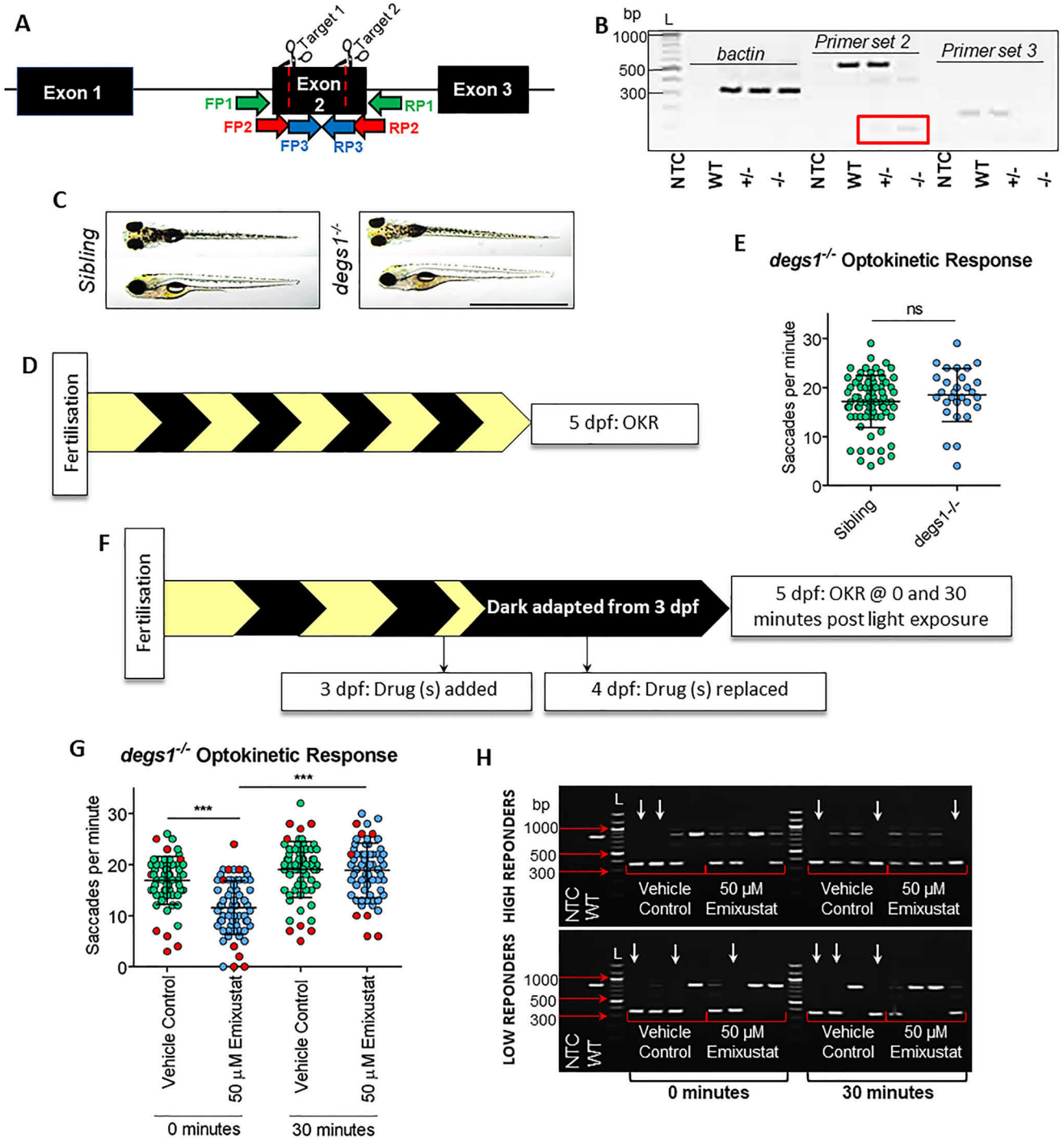

Figure 7. Des1 knockout does not eliminate cone photopic vision in zebrafish at 5 dpf. *A,* CRISPR/Cas9 knockout strategy of *degs1* in zebrafish. Both guides were targeted to exon 2 to induce a 484-bp deletion in the *degs1* gene that contains three exons in total. Forward primer 1 (*FP1*) to reverse primer 1 (*RP1*) amplifies an 807-bp genomic DNA WT product or a 323-bp product when deletion is present. For mRNA expression analysis, we used forward primer 2 (*FP2*) to reverse primer 2 (*RP2*), which span the deletion and amplify a 537-bp WT product or 61 bp when the deletion is present. Forward primer 3 (*FP3*) to reverse primer 3 (*RP3*) is nested within the deletion and amplifies a 162-bp WT product. *B,* agarose gel (1.5%) depicting *degs1* expression in WT, *degs1*$^{+/-}$ or *degs*$^{-/-}$ zebrafish. *L* = 100-bp ladder. *Red box* highlights the 61-bp product expected following a deletion event with primer set 2 in *degs1*$^{+/-}$ or *degs1*$^{-/-}$ samples. *C,* dorsal and lateral bright-field microscopy images of untreated *degs1* sibling (*degs1*$^{+/+}$ or *degs1*$^{+/-}$) and *degs1*$^{-/-}$ larvae at 5 dpf. *Scale bar* = 2 mm. *D,* schematic representation of experimental workflow. *degs1*$^{-/-}$ larvae were incubated under standard lighting conditions (14 h light and 10 h dark) until OKR analysis at 5 dpf. *E,* OKR of *degs1*$^{-/-}$ and sibling larvae at 5 dpf larvae following standard 14-h light and 10-h dark conditions. Data were analyzed by an unpaired, two-tailed *t* test, where *ns* = not significant ($p > 0.05$). $n \geq 30$ larvae with three independent biological replicates. *F,* schematic representation of experimental workflow. Des1$^{-/-}$ larvae were treated initially with 50 μM emixustat at 3 dpf, and drug was replaced at 4 dpf. Larvae were incubated under dark conditions until analysis at 5 dpf. *G,* at 5 dpf, a mixed population of *degs1*$^{-/-}$ and unaffected sibling larvae were subjected to OKR immediately following dark adaptation (0 min) or following 30 min of light (30 min). *Red points* denote the larvae genotyped following OKR. Data were analyzed by an unpaired, two-tailed *t* test, where *ns* = not significant and *** = $p < 0.001$. $n = 64$ larvae per group with two independent biological replicates. *H,* agarose gel (1.5%) highlighting genotypes of high/low-responding larvae in OKR assay. *White arrows* denote *degs1*$^{-/-}$ larvae. Eight larvae were genotyped per group (×4 "*low responders*" and ×4 "*high responders*"). *L* = 100-bp ladder.

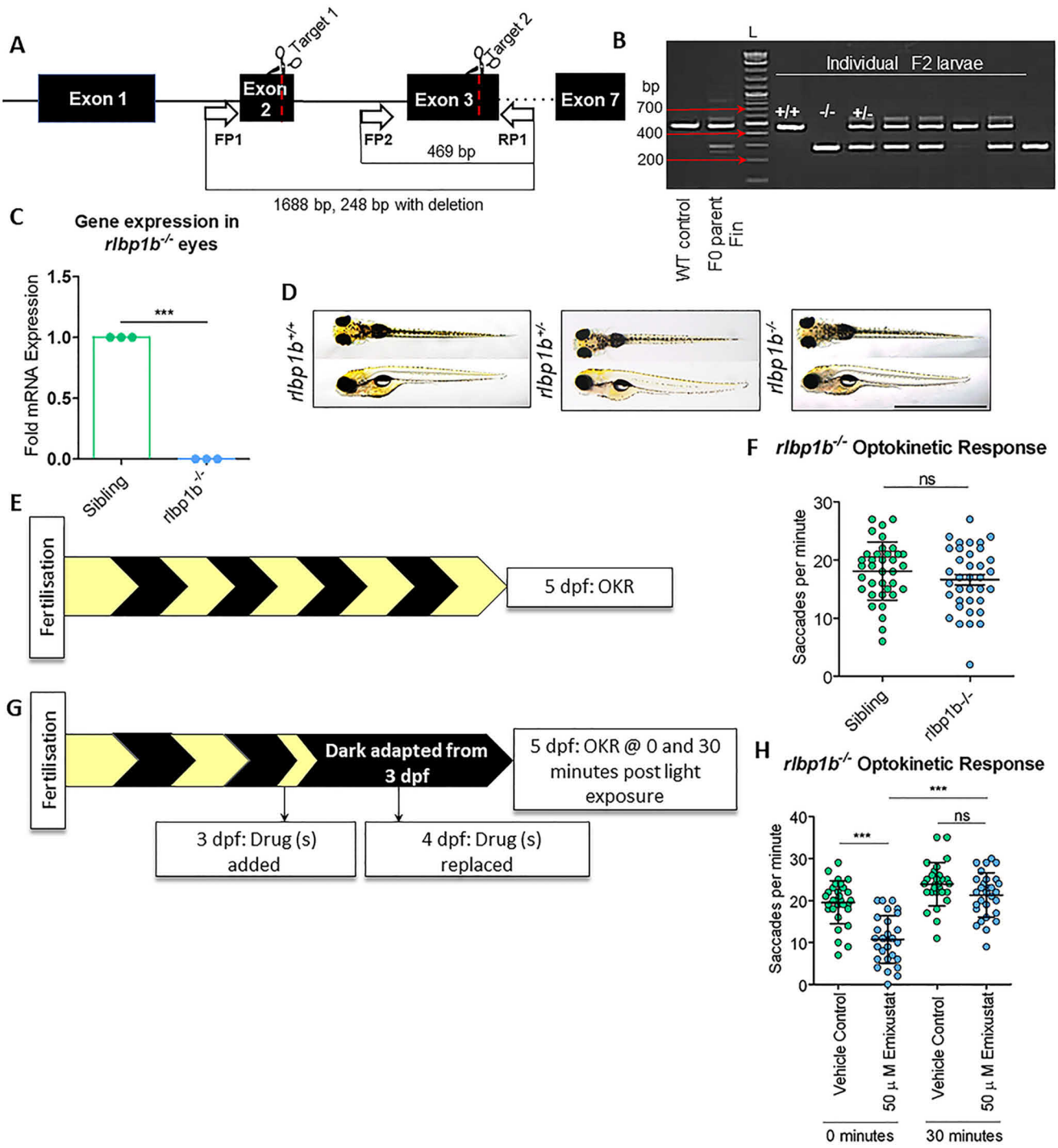

Figure 8. Knockout of RPE-expressed *rlbp1b* does not eliminate cone photopic vision in zebrafish at 5 dpf. *A,* CRISPR/Cas9 knockout strategy of RPE-expressed *rlbp1b*. Guides were targeted to exon 2 and exon 3 to induce a 1440-bp deletion in *rlbp1b* that contains seven exons. Forward primer 1 (*FP1*) to reverse primer 1 (*RP1*) amplifies a 1688-bp WT product or a 248-bp product when deletion is present. A poison forward primer (*FP2)* was designed in the middle of the deleted region to amplify a 469-bp WT product. *B,* agarose gel (1.5%) depicting the presence of the deletion in individual F2 larval genomic DNA. A WT control was used to amplify the upper band (469 bp), and gDNA from the injected F0 parent fin was used as a positive control to amplify both upper and lower bands (*mosaic*). *L* = 100-bp ladder. *C,* gene expression analysis of *rlbp1b* in *rlbp1b*$^{-/-}$ eyes. Data were analyzed by an unpaired, two-tailed *t* test, where *** = $p < 0.001$. Three independent biological replicates were performed with at least 10 larvae per replicate. *D,* dorsal and lateral bright-field microscopy images of untreated WT, *rlbp1b*$^{+/-}$, and *rlbp1b*$^{-/-}$ larvae at 5 dpf. *Scale bar* = 2 mm. *E,* schematic representation of experimental workflow. Rlbp1b$^{-/-}$ larvae were incubated under standard lighting conditions (14 h light and 10 h dark) until OKR analysis at 5 dpf. *F,* late photopic vision was measured by OKR in 5 dpf larvae. Data were analyzed by an unpaired, two-tailed *t* test, where *ns* = not significant ($p > 0.05$). $n = 36$ larvae with three independent biological replicates. *G,* schematic representation of experimental workflow. Rlbp1b$^{-/-}$ larvae were treated initially with 50 μM emixustat at 3 dpf, and drug was replaced at 4 dpf. Larvae were incubated under dark conditions until analysis at 5 dpf. *H,* at 5 dpf larvae were subjected to OKR immediately following dark adaptation (*0 min*) or following 30 min of light (30 min). Data were analyzed by an unpaired, two-tailed *t* test, where *ns* = not significant and *** = $p < 0.001$. $n = 36$ larvae with three independent biological replicates.

merases to photopic vision (i) immediately following dark adaptation, (ii) after 30 min of light, or (iii) after ~4–6 h of light. We exploited emixustat for its chemical ability to scavenge retinal and to inhibit the RPE65 isomerase (26). Likewise, fenretinide causes depletion of vitamin A by disrupting the retinol-dependent binding of RBP4 to transthyretin (35), and it also inhibits the DES1 isomerase (31–33). A1120 is a more-selective RBP4 antagonist.

Immediate and late cone photopic vision depend on different visual cycle pathways

The ray-finned fish lineage, including zebrafish, underwent whole-genome duplication resulting in two paralogues of many teleost genes (46). In zebrafish, Rpe65a is exclusively expressed in the RPE, whereas a contentious Rpe65c isoform was localized to retinal Müller glia (39). Based on this expression pattern and the requirement of mammalian cones on both the RPE and intraretinal visual cycles for complete dark adaptation (47), we predicted that emixustat could impair both immediate and possibly also early/late cone-based vision. Although emixustat inhibited cone responses immediately following exposure to light, treated larvae had normal OKR responses after prolonged light exposure. This agrees with previous genetic studies demonstrating OKR contrast sensitivity is unaffected in Rpe65a knockdown larvae raised under normal lighting conditions (20), but implicates RPE-specific Rpe65a in immediate photopic vision after dark adaptation. However, we cannot unequivocally exclude a role for zebrafish Rpe65c in Müller glia in the immediate response.

Retinoid profiles are altered in dark-adapted zebrafish larvae treated with visual cycle isomerase inhibitors

Retinoid analysis from dark-adapted zebrafish larvae show reduced 11-*cis*-retinoids (11cROL, 11cRAL, and 11cRP) with emixustat treatment. Fenretinide also dose-dependently suppressed immediate photopic vision. However, although 11-*cis*-retinoid levels were lower in fenretinide-treated *versus* vehicle-treated larvae, the degree of suppressed vision was less than with emixustat. Levels of atROL, atRAL, and atRP were also suppressed in fenretinide-treated *versus* vehicle-treated larvae, an effect not observed in emixustat-treated larvae.

Exogenous 9cRAL supplementation restores immediate photopic vision following visual cycle inhibition

Treatment with exogenous 9cRAL recovers ERG responses in *Rpe65*$^{-/-}$ mice and functional vision in *Rpe65*-deficient dogs, establishing its potential as a chromophore replacement therapy (30, 47, 48). In agreement, immediate photopic vision significantly improved emixustat and/or fenretinide-treated larvae supplemented with 9cRAL. Thus, the impaired cone vision we observe is a specific pharmacological effect on the visual cycle and not a result of ocular toxicity. Additionally, fenretinide-treated larvae display impaired immediate photopic vision despite relatively high 11cRAL levels. The improvement of vision with exogenous 9cRAL suggests that the 11cRAL stores present may be unavailable to cones in fenretinide-treated larvae. Improved vision in emixustat-treated larvae supplemented with 9cRAL was not coupled to increased 11cRAL levels. Instead, all 9-*cis*-retinoid profiles (9cRAL, 9cROL, and 9cRP) were significantly increased, indicating that the recovered vision may be mediated by iso-opsins.

Differential requirements of Rpe65 for immediate and early cone-based photopic vision

Because emixustat did not affect late photopic vision in zebrafish, we investigated whether impaired immediate photopic vision in dark-adapted animals could recover in a light-dependent, Rpe65-independent manner. Pharmacological RPE65 inhibition significantly reduces 11cRAL levels in multiple models, *e.g.* by Ret-NH_2 in zebrafish (20), by emixustat in mice (26), and by emixustat or fenretinide in *ex vivo* RPE microsomes (32). Here, as expected, dark-adapted, WT larvae treated with emixustat display an ~10-fold reduction in 11cRAL. Interestingly, 11cRAL levels did not recover following 30 min of light exposure despite recovery of early photopic vision. A reduction in total retinoid was observed indicating that emixustat may be trapping atRAL and forming unknown or undetectable conjugates. Consistent with light overcoming emixustat-mediated visual impairment, atRAL was restored to levels similar to vehicle controls 30 min following light exposure, consistent with initiation of phototransduction. However, that photopic vision recovers in the light, surmounting emixustat, without an associated increase in 11cRAL levels is intriguing. Potentially, the small amount of 11cRAL available to the photopic cycle activates cone opsins in a steady state and is sufficient to sustain a stable visual response during this 30-min light exposure. As retinyl esters support cone function (49) and are a significant source for cone pigment regeneration (50), one possibility is that 11cRP reserves were utilized upon exposure to light. However, in line with previous studies employing RPE65 inhibitors in zebrafish (49), emixustat treatment completely blocked generation of 11cRP both in the dark and light. An alternative RPE65-independent isomerization event for cone pigment regeneration was recently described in mice (18). This cone regeneration mechanisms involves Müller glia-expressed RGR-opsin, which converts atROL to 11cROL upon visible light exposure. In RPE cells, RGR opsin also affects light-dependent mobilization of atREs, suggesting it diverts substrate away from RPE65 in RPE cells toward the Müller cell visual cycle (51).

Using genetic and pharmacological approaches, we investigate the molecular mechanisms mediating this 30-min switch from a light-independent visual cycle, supporting immediate photopic vision, to a light-dependent visual cycle, supporting early photopic vision. When WT larvae were treated with the potent RBP4 antagonist A1120 alone, immediate photopic vision was reduced, but recovery of early photopic vision was equivalent to vehicle controls. This indicates that RBP4 is required for the nonphotopic visual cycle but not for the photopic visual cycle. Furthermore, knockout of *degs1*$^{-/-}$ in zebrafish showed no modulation of immediate, early, or late photopic vision suggesting Des1 is not essential for either the photopic or nonphotopic visual cycles. The phenotypic differences between Des1 pharmacological inhibition and the genetic knockout model may be attributed to polypharmacology or genetic compensation and illustrates the importance of applying complementary approaches in parallel. Mammalian

CRALBP forms a complex with DES1 (15) and is reported to regulate the cone visual cycle. Deletion of CRALBP in mice results in reduced photopic ERG responses (52). Adenovirus-mediated delivery of Müller cell CRALBP restored cone-driven responses. Here, knockout of the RPE-expressed *rlbp1b* paralogue in zebrafish did not eliminate immediate or early photopic vision in larvae treated with emixustat. All studies reported here employ standard OKR conditions (*i.e.* 1 cm stripes with 99% contrast) in 5 dpf larvae. Future investigations at older ages or using more sophisticated contrast sensitivity or visual acuity behavioral assays may unveil more subtle visual defects following pharmacological or genetic perturbations.

Significantly, fenretinide and emixustat hydrochloride have reached phases II and III clinical trials, respectively, for use in geographic atrophy. Night blindness and dry eye are side effects of fenretinide treatment (53). Our data demonstrate that fenretinide also impairs photopic vision; thus, concerns arise over potential adverse drug reactions in the clinic with fenretinide use to treat diseases such as geographic atrophy, cancer, acne, cystic fibrosis, and psoriasis. Likewise, emixustat is now in phase III clinical trial for the inherited retinal degeneration Stargardt disease with the intention of suppressing retinoid cycling (37). We show that the photopic visual cycle overcomes emixustat, which may have significant impact on clinical outcomes.

In summary, pharmacological and genetic models of visual cycle modulation enhanced our knowledge of the fundamental mechanisms of cone photopic vision. Differential stages of vertebrate photopic vision demand differential biochemical pathways, in light and dark. Rpe65 regenerates photopigment required by cones for immediate photopic response. In contrast, during sustained light, Rpe65 appears redundant to a light-dependent regeneration of visual pigments, a process whereby diminished 11cRAL levels are sufficient for photopic vision.

Experimental procedures

Zebrafish breeding and maintenance

Adult zebrafish were maintained in a 14-hour light, 10-hour dark cycle in a recirculating water system at 28 °C. Annual facility environmental parameters are published online (54).

WT (Tübingen) larvae were generated through natural spawning. Larvae were raised at 28 °C in embryo medium (0.137 M NaCl, 5.4 mM KCl, 5.5 mM Na_2HPO_4, 0.44 mM KH_2PO_4, 1.3 mM $CaCl_2$, 1.0 mM $MgSO_4$, and 4.2 mM $NaHCO_3$) containing methylene blue (Sigma-Aldrich, UK).

Ethics statement

All experiments with zebrafish larvae were performed according to ethical exemptions granted by the UCD Animal Research Ethics Committee, University College Dublin (AREC-Kennedy), and the Health Products Regulatory Authority (Project Authorization AE18982/P062).

Generation of mutant zebrafish

Custom crRNA guides, containing an NGG protospacer adjacent motif (PAM) were designed per gene using Benchling (RRID:SCR_013955) CRISPR guide software. All guide sequences and PAMs are listed in Table S1. The Alt-R system (Integrated DNA Technologies) was used to knock out *rlbp1b* and *degs1* in zebrafish. Briefly, 36 ng/μl crRNA and 67 ng/μl tracrRNA were complexed in nuclease-free duplex buffer by heating to 95 °C for 10 min. Sample was cooled to room temperature, and a final working concentration of 0.5 μg/μl *Streptococcus pyogenes* Cas9 nuclease (Integrated DNA Technologies) was added. The mixture was heated to 37 °C for 15 min before microinjection into WT embryos at one-cell stage. Injected fish were raised until adulthood and outcrossed to screen for germline transmission of the null target gene. Isogenic F_1 heterozygous adult fish were incrossed to generate homozygous F_2 mutants.

Genomic DNA extraction and PCR

DNA was extracted from injected F0 or germline F2 *rlbp1b*$^{-/-}$ larvae by boiling the sample at 95 °C in NaOH (50 mM) (Sigma-Aldrich, UK) before neutralizing with 1/10th Trizma (Tris base) (Sigma-Aldrich, UK). The region of interest was amplified by PCR using the following primers, which span the *rlbp1b* or *degs1* mutation site: *rlbp1b,* 5′-CCACAGAGTGGAACATTTCGA-3′, 5′-GATGATGCAACACTATTGCCCA-3′, and 5′-ACCTTTCAGCATTCACAATCCT-3′; *degs1,* 5′-TTCTCCATGACCTTTCAGCCC-3′ and 5′-TGCTCTCACCATTGGTAGTCG-3′. Fragment sizes were run on a 1.5% agarose gel and compared against a 100-bp DNA ladder (New England Biolabs, UK).

Total RNA extraction, cDNA synthesis, and RT-PCR/qPCR

At 5 dpf, ~20–50 eyes (10–25 larvae) were enucleated and stored in RNAlater (Qiagen, Germany) individually at 4 °C. Larval trunks were genotyped as described previously. Eyes were pooled, and total RNA was extracted using mirVana™ miRNA isolation kit (Thermo Fisher Scientific) as per the manufacturer's instructions. NaOAc (3 M) and 100% ethanol were added to the eluted RNA, vortexed, and left overnight at −20 °C. Samples were centrifuged at 14,000 rpm for 60 min at 4 °C; the supernatant was removed before the pellet was resuspended in 80% ethanol and centrifuged for a further 60 min at 14,000 rpm. Supernatant was discarded, and the pellet was resuspended in ultrapure water. Total RNA concentration was quantified at 260 nm (Spectrophotometer ND-1000), and samples were stored at −80 °C until further use. cDNA was synthesized using PrimeScript™ RT reagent kit (Perfect Real Time) (TAKARA, Japan). qRT-PCRs were made up on ice with 0.2 μl of forward and reverse primers (*rlbp1b,* 5′-TGAGCTTGCTAAAGGTGTTCAGG-3′ and 5′-TCAGGATAATCCCGTCTGAAGC-3′), 5 μl of SYBR Green Master Mix (Thermo Fisher Scientific), 3.6 μl of RNase-free water, and 1 μl of cDNA template (12.5 ng) were added per sample. qRT-PCR cycles were carried out using the following parameters: 50 °C for 2 min, 95 °C for 10 min, and 95 °C for 15 s with 40 repeats and 60 °C for 1 min on a Quant Studio 7 Flex Real-Time PCR system. To evaluate *degs1* expression, the cDNA was amplified by RT-PCR using the following primer sets: *degs1* forward 2, 5′-GTCAGCACGATGGTGGTGTC-3′, and *degs1* reverse 2, 5′-TGGAGACCCATGCCCAGCAT-3′; *degs1* forward 3, 5′-GGACGTGGACATCCCCAC-

TGA-3′, and *degs1* reverse 3, 5′-AGCTGGATGGCCACGTTCAG-3′. Samples were run on a 1.5% agarose gel and compared against a 100-bp DNA ladder (New England Biolabs, UK).

Drug preparation and treatment

WT, Rlbp1b, and Des1 larvae were raised from embryos under standard 14-h light and 10-h dark conditions. At 3 dpf, five larvae per well were placed in 48-well cell culture plates (Greiner Bio-one, Austria). Emixustat hydrochloride (Medchem), fenretinide (Cayman Chemical), and A1120 (Sigma-Aldrich, UK) were prepared in embryo medium, and 400 μl of drug solution at 1–50 μM in 0.01–0.5% DMSO was added to the wells. For emixustat and fenretinide combinations, 1–10 μM fenretinide was added 15 min prior to the addition of 50 μM emixustat. Larvae were initially treated at 74–76 hpf, and the drug was replaced at 98–100 hpf. Four hours following primary drug treatment (*i.e.* 78–80 and 102–104 hpf), 10 μM 9-*cis*-retinal (Sigma-Aldrich, UK) was added to the embryo medium. Exogenous 9-*cis*-retinal was handled under dim red light.

Visual behavior analysis

To measure OKR, single larvae were immobilized in prewarmed 9% methylcellulose (Sigma-Aldrich, UK) and placed in the center of a rotating drum containing 20 vertical, 1 cm thick black and white stripes. The angle subtended was 0.58 rad (33.7°). The drum was rotated at 18 rpm for 30 s in a clockwise direction and 30 s in a counterclockwise direction. Saccadic eye movements per min were recorded manually. All OKR measurements were performed in larvae at 5 dpf between 10 a.m. (ZT 2.5) and 2 p.m. (ZT 6.5).

Histological analysis

Larvae were fixed in glass vials containing 2.5% glutaraldehyde, 2% paraformaldehyde, and 0.1% Sorenson's phosphate buffer (pH 7.3) and were placed at 4 °C. Samples were washed before post-fixation in 1% osmium tetroxide (Sigma-Aldrich, UK) and dehydrated using an ethanol gradient (30, 50, 70, 90, and 100%). Samples were transferred to propylene oxide (Sigma-Aldrich, UK) and embedded in agar epoxy resin overnight, and 0.5-μm sections were cut using an ultramicrotome (Leica EM UC6). Sections were placed on glass slides and stained with toluidine blue (Sigma-Aldrich, UK) for 30–60 s and imaged using a Leica DMLB bright-field illumination microscope with a Leica DFC 480 camera attachment.

For transmission EM, 0.08-μm sections were cut using a diamond knife and a Leica EM UC6 ultramicrotome. Sections were transferred to a support grid, stained with uranyl acetate and lead citrate, and imaged on a FEI-Tecnai 12 BioTwin transmission electron microscope (FEI Electron Optics).

Drug-treated larvae were fixed at 5 dpf with 4% paraformaldehyde (Sigma-Aldrich, UK). Larvae were cryoprotected in a sucrose series before embedding in optimal cutting temperature (OCT) medium (VWR International). Sections were cut to 14 μm and thaw-mounted onto charged Superfrost plus slides (Thermo Fisher Scientific). Sections were rehydrated using 1× PBS supplemented with Tween 20 (Sigma-Aldrich, UK) (0.01% PBST) before blocking in 10% goat serum (Sigma-Aldrich, UK) for 1 h. Monoclonal zpr-1 was used at 1:200 (Zebrafish International Resource Center, Eugene, OR). Slides were washed before incubating with the secondary antibody (Alexa Fluor 488 anti-mouse IgG). Primary and secondary antibodies were diluted in blocking solution. Slides were mounted using Vectashield (Vector Laboratories) before imaging using a Zeiss LSM510 confocal microscope (Carl Zeiss AG, Germany) with a ×63 objective.

Retinoid quantification

For retinoid analysis, 105 larvae per treatment condition at 5 dpf were euthanized in ice water before their heads were collected under dim red light. For normal-phase HPLC analysis of retinoids, all retinoid extractions were carried out under dim red light in a dark room. Zebrafish heads were stored at −80 °C, thawed on ice, and homogenized in 500 μl of phosphate-buffered saline (PBS) using a glass tissue grinder (Kontes). Protein concentration was determined using 50 μl of sample and a Micro BCA protein assay kit (Pierce). To the remaining 450 μl of homogenate, 25 μl of 5% SDS (~0.2% SDS final concentration) and 50 μl of brine were added, and samples were briefly mixed. Hydroxylamine hydrochloride (500 μl of 1.0 M solution in pH 7.0 PBS) was added to generate retinal oxime, and samples were vortexed and incubated at room temperature for 15 min. The aqueous phase was quenched and diluted using 2 ml of cold methanol. The samples were twice extracted by addition of 2-ml aliquots of hexane, brief vortexing, and centrifugation at 3000 × *g* for 5 min to separate the phases. Pooled hexane extracts were added to 13 × 100-mm borosilicate test tubes and evaporated to dryness under a stream of nitrogen. Dried samples were dissolved in 100 μl of hexane and analyzed by normal-phase HPLC using an Agilent 1100 series chromatograph equipped with a Supelcosil LC-Si column (4.6 × 250 mm, 5 μm) using a 0.2–10% dioxane gradient in hexane at a flow rate of 2 ml per min. The eluted mobile phase was analyzed using a photodiode-array detector. Spectra (210–450 nm) were acquired for all eluted peaks. The identity of eluted peaks was established by comparison with spectra and elution times of known authentic retinoid standards. Retinoid amounts were quantitated by comparing their respective peak areas to calibration curves established with retinoid standards.

Photostability of emixustat hydrochloride

Liquid chromatography used a Dionex Ultimate 3000 RSLC micro-LC system (Thermo Fisher Scientific). Separation was performed using a Thermo Acclaim RSLC 120 2.2-μm, 120 Å, 1.0 × 100-mm LC column (Thermo Fisher Scientific). LC parameters were as follows: elution mode, gradient (from 90% A to 90% B in 15 min); flow rate, 45 μl/min; column temperature, 3 °C; detector wavelength, 230 nm; and injection volume, 2 μl. Mobile phases were as follows: A, H_2O + 0.1% formic acid (v/v); B, acetonitrile + 0.1% FA (v/v). Mass spectrometry analysis was performed using an LTQ-XL–Orbital-XL (Thermo Fisher Scientific) equipped with HESI II ESI ion source. Source parameters were as follows: ion spray voltage (V), 4.6; capillary temperature (°C), 280; sheath gas, flow gas flow (Arb), 20; and auxiliary gas flow (Arb), 8. Resolution was set to 30,000 in FT mode, and mass range set to 150–500 Da in positive-ion mode. Peak area of emixustat-protonated mass was calculated and

recorded using Xcalibur software (version 2.21). The protonated mass ions were identified using an error tolerance of 5 ppm for their corresponding theoretical monoisotopic mass.

For nuclear magnetic resonance (NMR) analysis, emixustat (7 mg) was dissolved in DMSO-d_6 (600 μl) under dim red light and covered with aluminum foil until ^{1}H NMR and HSQC experiments were performed. The NMR tube was exposed to visible light for 30 min, followed by a repeat NMR analysis. ^{1}H NMR spectra were measured in DMSO-d6 at 400 MHz. Chemical shifts (δ) are quoted in parts per million (ppm) referenced to residual solvent peak (*e.g.* DMSO-d_6: ^{1}H, 2.50 and 3.33 ppm).

Statistical analysis

Statistical analysis was performed using GraphPad Prism™ software (GraphPad, San Diego, CA). A two-tailed Student's unpaired *t* test was applied comparing two experimental groups. For analysis involving more than two independent groups, a one-way ANOVA and Dunnett's multiple comparison test or Bonferroni post hoc test were performed. Experiments composed of two variables were tested for significance using a two-way ANOVA and a Bonferroni post hoc test. All data are presented as mean ± S.D. Statistical significance was assigned to the following p values: * = $p < 0.05$, ** = $p < 0.01$, and *** = $p < 0.001$.

Data availability

Raw data supporting the findings of this study are available from the corresponding author on request.

Author contributions—R. W. and B. N. K. conceptualization; R. W. data curation; R. W. and B. N. K. formal analysis; R. W., J. J. K., D. F. C., D. A. P., E. M. M., G. H. T., and B. N. K. Validation; R. W., J. J. K., D. F. C., D. A. P., and E. M. M. investigation; R. W. and B. N. K. methodology; R. W. and B. N. K. writing-original draft; R. W., S. E. B., J. B. H., G. H. T., and B. N. K. writing-review and editing; G. H. T. and B. N. K. resources; B. N. K. supervision; B. N. K. project administration; R. W. performed visual function analysis, drug treatment optimization, retinal histology experiments, gene expression analysis, genotyping, prepared samples for retinoid analysis and created degs1 and rlbp1b knockout zebrafish; J. J. K. performed retinoid analysis; D. F. C. performed mass spectrometry analysis of emixustat; D. A. P. and E. M. M. performed Nuclear Magnetic Resonance analysis of emixustat; R. W., S. E. B., J. B. H., G. H. T., and B. N. K. interpreted the results and provided significant intellectual input.

Acknowledgments—We thank the UCD Biomedical Facility technicians for zebrafish maintenance and the UCD Conway Institute Imaging Core, with particular thanks to Dr. Dimitri Scholz and Dr. Niamh Stephens. We wish to acknowledge our Public and Patient Involvement panel and Fighting Blindness for providing meaningful insights into this project and Research to Prevent Blindness unrestricted grant (to the Jules Stein Eye Institute). We thank Prof. Jack Saari for helpful discussions surrounding this project and Dr. Ross Collery for proof-reading the manuscript.

References

1. Saari J. C. (2016) Vitamin A and Vision. In *The Biochemistry of Retinoid Signaling II: Subcellular Biochemistry* (Asson-Batres M. and Rochette-Egly C. eds), vol 81, pp. 231–259, Springer, Dordrecht
2. Mata, N. L., Moghrabi, W. N., Lee, J. S., Bui, T. V., Radu, R. A., Horwitz, J., and Travis, G. H. (2004) Rpe65 is a retinyl ester binding protein that presents insoluble substrate to the isomerase in retinal pigment epithelial cells. *J. Biol. Chem.* **279,** 635–643 CrossRef Medline
3. Redmond, T. M., Poliakov, E., Yu, S., Tsai, J. Y., Lu, Z., and Gentleman, S. (2005) Mutation of key residues of RPE65 abolishes its enzymatic role as isomerohydrolase in the visual cycle. *Proc. Natl. Acad. Sci. U.S.A.* **102,** 13658–13663 CrossRef Medline
4. Moiseyev, G., Chen, Y., Takahashi, Y., Wu, B. X., and Ma, J. X. (2005) RPE65 is the isomerohydrolase in the retinoid visual cycle. *Proc. Natl. Acad. Sci. U.S.A.* **102,** 12413–12418 CrossRef Medline
5. Fan, J., Rohrer, B., Frederick, J. M., Baehr, W., and Crouch, R. K. (2008) Rpe65$^{-/-}$ and Lrat$^{-/-}$ mice: comparable models of leber congenital amaurosis. *Invest. Ophthalmol. Vis. Sci.* **49,** 2384–2389 CrossRef Medline
6. Fan, J., Rohrer, B., Moiseyev, G., Ma, J. X., and Crouch, R. K. (2003) Isorhodopsin rather than rhodopsin mediates rod function in RPE65 knock-out mice. *Proc. Natl. Acad. Sci. U.S.A.* **100,** 13662–13667 CrossRef Medline
7. O'Byrne, S. M., Wongsiriroj, N., Libien, J., Vogel, S., Goldberg, I. J., Baehr, W., Palczewski, K., and Blaner, W. S. (2005) Retinoid absorption and storage is impaired in mice lacking lecithin:retinol acyltransferase (LRAT). *J. Biol. Chem.* **280,** 35647–35657 CrossRef Medline
8. Redmond, T. M., Yu, S., Lee, E., Bok, D., Hamasaki, D., Chen, N., Goletz, P., Ma, J. X., Crouch, R. K., and Pfeifer, K. (1998) Rpe65 is necessary for production of 11-cis-vitamin A in the retinal visual cycle. *Nat. Genet.* **20,** 344–351 CrossRef Medline
9. Mata, N. L., Radu, R. A., Clemmons, R. C., and Travis, G. H. (2002) Isomerization and oxidation of vitamin a in cone-dominant retinas: a novel pathway for visual-pigment regeneration in daylight. *Neuron* **36,** 69–80 CrossRef Medline
10. Goldstein, E. B. (1970) Cone pigment regeneration in the isolated frog retina. *Vision Res.* **10,** 1065–1068 CrossRef Medline
11. Hood, D. C., and Hock, P. A. (1973) Recovery of cone receptor activity in the frog's isolated retina. *Vision Res.* **13,** 1943–1951 CrossRef Medline
12. Wang, J. S., and Kefalov, V. J. (2009) An alternative pathway mediates the mouse and human cone visual cycle. *Curr. Biol.* **19,** 1665–1669 CrossRef Medline
13. Wang, J. S., and Kefalov, V. J. (2011) The cone-specific visual cycle. *Prog. Retin. Eye Res.* **30,** 115–128 CrossRef Medline
14. Mata, N. L., Ruiz, A., Radu, R. A., Bui, T. V., and Travis, G. H. (2005) Chicken retinas contain a retinoid isomerase activity that catalyzes the direct conversion of all-*trans*-retinol to 11-cis-retinol. *Biochemistry* **44,** 11715–11721 CrossRef Medline
15. Kaylor, J. J., Yuan, Q., Cook, J., Sarfare, S., Makshanoff, J., Miu, A., Kim, A., Kim, P., Habib, S., Roybal, C. N., Xu, T., Nusinowitz, S., and Travis, G. H. (2013) Identification of DES1 as a vitamin A isomerase in Müller glial cells of the retina. *Nat. Chem. Biol.* **9,** 30–36 CrossRef Medline
16. Kiser, P. D., Kolesnikov, A. V., Kiser, J. Z., Dong, Z., Chaurasia, B., Wang, L., Summers, S. A., Hoang, T., Blackshaw, S., Peachey, N. S., Kefalov, V. J., and Palczewski, K. (2019) Conditional deletion of Des1 in the mouse retina does not impair the visual cycle in cones. *FASEB J.* **33,** 5782–5792 CrossRef Medline
17. Chen, P., Hao, W., Rife, L., Wang, X. P., Shen, D., Chen, J., Ogden, T., Van Boemel, G. B., Wu, L., Yang, M., and Fong, H. K. (2001) A photic visual cycle of rhodopsin regeneration is dependent on Rgr. *Nat. Genet.* **28,** 256–260 CrossRef Medline
18. Morshedian, A., Kaylor, J. J., Ng, S. Y., Tsan, A., Frederiksen, R., Xu, T., Yuan, L., Sampath, A. P., Radu, R. A., Fain, G. L., and Travis, G. H. (2019) Light-driven regeneration of cone visual pigments through a mechanism involving RGR opsin in Müller glial cells. *Neuron* **102,** 1172–1183.e5 CrossRef Medline
19. Bainbridge, J. W., Smith, A. J., Barker, S. S., Robbie, S., Henderson, R., Balaggan, K., Viswanathan, A., Holder, G. E., Stockman, A., Tyler, N., Petersen-Jones, S., Bhattacharya, S. S., Thrasher, A. J., Fitzke, F. W., Carter, B. J., *et al.* (2008) Effect of gene therapy on visual function in Leber's congenital amaurosis. *N. Engl. J. Med.* **358,** 2231–2239 CrossRef Medline
20. Schonthaler, H. B., Lampert, J. M., Isken, A., Rinner, O., Mader, A., Gesemann, M., Oberhauser, V., Golczak, M., Biehlmaier, O., Palczewski, K., Neuhauss, S. C., and von Lintig, J. (2007) Evidence for RPE65-independent vision in the cone-dominated zebrafish retina. *Eur. J. Neurosci.* **26,** 1940–1949 CrossRef Medline

21. Bilotta, J., Saszik, S., and Sutherland, S. E. (2001) Rod contributions to the electroretinogram of the dark-adapted developing zebrafish. *Dev. Dyn.* **222,** 564–570 CrossRef Medline
22. Saszik, S., Bilotta, J., and Givin, C. M. (1999) ERG assessment of zebrafish retinal development. *Vis. Neurosci.* **16,** 881–888 CrossRef Medline
23. Collery, R., McLoughlin, S., Vendrell, V., Finnegan, J., Crabb, J. W., Saari, J. C., and Kennedy, B. N. (2008) Duplication and divergence of zebrafish CRALBP genes uncovers novel role for RPE- and Muller-CRALBP in cone vision. *Invest. Ophthalmol. Vis. Sci.* **49,** 3812–3820 CrossRef Medline
24. Fleisch, V. C., Schonthaler, H. B., von Lintig, J., and Neuhauss, S. C. (2008) Subfunctionalization of a retinoid-binding protein provides evidence for two parallel visual cycles in the cone-dominant zebrafish retina. *J. Neurosci.* **28,** 8208–8216 CrossRef Medline
25. Travis, G. H., Golczak, M., Moise, A. R., and Palczewski, K. (2007) Diseases caused by defects in the visual cycle: retinoids as potential therapeutic agents. *Annu. Rev. Pharmacol. Toxicol.* **47,** 469–512 CrossRef Medline
26. Zhang, J., Kiser, P. D., Badiee, M., Palczewska, G., Dong, Z., Golczak, M., Tochtrop, G. P., and Palczewski, K. (2015) Molecular pharmacodynamics of emixustat in protection against retinal degeneration. *J. Clin. Invest.* **125,** 2781–2794 CrossRef Medline
27. Boyer, N. P., Higbee, D., Currin, M. B., Blakeley, L. R., Chen, C., Ablonczy, Z., Crouch, R. K., and Koutalos, Y. (2012) Lipofuscin and *N*-retinylidene-*N*-retinylethanolamine (A2E) accumulate in retinal pigment epithelium in absence of light exposure: their origin is 11-cis-retinal. *J. Biol. Chem.* **287,** 22276–22286 CrossRef Medline
28. Cornwall, M. C., and Fain, G. L. (1994) Bleached pigment activates transduction in isolated rods of the salamander retina. *J. Physiol.* **480,** 261–279 CrossRef Medline
29. Woodruff, M. L., Wang, Z., Chung, H. Y., Redmond, T. M., Fain, G. L., and Lem, J. (2003) Spontaneous activity of opsin apoprotein is a cause of Leber congenital amaurosis. *Nat. Genet.* **35,** 158–164 CrossRef Medline
30. Van Hooser, J. P., Aleman, T. S., He, Y. G., Cideciyan, A. V., Kuksa, V., Pittler, S. J., Stone, E. M., Jacobson, S. G., and Palczewski, K. (2000) Rapid restoration of visual pigment and function with oral retinoid in a mouse model of childhood blindness. *Proc. Natl. Acad. Sci. U.S.A.* **97,** 8623–8628 CrossRef Medline
31. Siddique, M. M., Li, Y., Wang, L., Ching, J., Mal, M., Ilkayeva, O., Wu, Y. J., Bay, B. H., and Summers, S. A. (2013) Ablation of dihydroceramide desaturase 1, a therapeutic target for the treatment of metabolic diseases, simultaneously stimulates anabolic and catabolic signaling. *Mol. Cell. Biol.* **33,** 2353–2369 CrossRef Medline
32. Kiser, P. D., Zhang, J., and Sharma, A., Angueyra, J. M., Kolesnikov, A. V., Badiee, M., Tochtrop, G. P., Kinoshita, J., Peachey, N. S., Li, W., Kefalov, V. J., and Palczewski, K. (2018) Retinoid isomerase inhibitors impair but do not block mammalian cone photoreceptor function. *J. Gen. Physiol.* **150,** 571–590 CrossRef Medline
33. Rahmaniyan, M., Curley, R. W., Jr, Obeid, L. M., Hannun, Y. A., and Kraveka, J. M. (2011) Identification of dihydroceramide desaturase as a direct *in vitro* target for fenretinide. *J. Biol. Chem.* **286,** 24754–24764 CrossRef Medline
34. Motani, A., Wang, Z., Conn, M., Siegler, K., Zhang, Y., Liu, Q., Johnstone, S., Xu, H., Thibault, S., Wang, Y., Fan, P., Connors, R., Le, H., Xu, G., Walker, N., Shan, B., and Coward, P. (2009) Identification and characterization of a non-retinoid ligand for retinol-binding protein 4 which lowers serum retinol-binding protein 4 levels *in vivo*. *J. Biol. Chem.* **284,** 7673–7680 CrossRef Medline
35. Dobri, N., Qin, Q., Kong, J., Yamamoto, K., Liu, Z., Moiseyev, G., Ma, J. X., Allikmets, R., Sparrow, J. R., and Petrukhin, K. (2013) A1120, a nonretinoid RBP4 antagonist, inhibits formation of cytotoxic bisretinoids in the animal model of enhanced retinal lipofuscinogenesis. *Invest. Ophthalmol. Vis. Sci.* **54,** 85–95 CrossRef Medline
36. Rosenfeld, P. J., Dugel, P. U., Holz, F. G., Heier, J. S., Pearlman, J. A., Novack, R. L., Csaky, K. G., Koester, J. M., Gregory, J. K., and Kubota, R. (2018) Emixustat hydrochloride for geographic atrophy secondary to age-related macular degeneration: a randomized clinical trial. *Ophthalmology* **125,** 1556–1567 CrossRef Medline
37. Hussain, R. M., Ciulla, T. A., Berrocal, A. M., Gregori, N. Z., Flynn, H. W., Jr., and Lam, B. L. (2018) Stargardt macular dystrophy and evolving therapies. *Expert Opin. Biol. Ther.* **18,** 1049–1059 CrossRef Medline
38. Brockerhoff, S. E., Dowling, J. E., and Hurley, J. B. (1998) Zebrafish retinal mutants. *Vision Res.* **38,** 1335–1339 CrossRef Medline
39. Takahashi, Y., Moiseyev, G., Chen, Y., Nikolaeva, O., and Ma, J.-X. (2011) An alternative isomerohydrolase in the retinal Müller cells of a cone-dominant species. *FEBS J.* **278,** 2913–2926 CrossRef Medline
40. Ward, R., Ali, Z., Slater, K., Reynolds, A. L., Jensen, L. D., and Kennedy, B. N. (2020) Pharmacological restoration of visual function in a zebrafish model of von-Hippel Lindau disease. *Dev. Biol.* **457,** 226–234 CrossRef Medline
41. Daly, C., Shine, L., Heffernan, T., Deeti, S., Reynolds, A. L., O'Connor, J. J., Dillon, E. T., Duffy, D. J., Kolch, W., Cagney, G., and Kennedy, B. N. (2017) A brain-derived neurotrophic factor mimetic is sufficient to restore cone photoreceptor visual function in an inherited blindness model. *Sci. Rep.* **7,** 11320 CrossRef Medline
42. Saari, J. C., Nawrot, M., Garwin, G. G., Kennedy, M. J., Hurley, J. B., Ghyselinck, N. B., and Chambon, P. (2002) Analysis of the visual cycle in cellular retinol-binding protein type I (CRBPI) knockout mice. *Invest. Ophthalmol. Vis. Sci.* **43,** 1730–1735 Medline
43. Saari, J. C., Nawrot, M., Kennedy, B. N., Garwin, G. G., Hurley, J. B., Huang, J., Possin, D. E., and Crabb, J. W. (2001) Visual cycle impairment in cellular retinaldehyde binding protein (CRALBP) knockout mice results in delayed dark adaptation. *Neuron* **29,** 739–748 CrossRef Medline
44. Kolesnikov, A. V., Tang, P. H., and Kefalov, V. J. (2018) Examining the role of cone-expressed RPE65 in mouse cone function. *Sci. Rep.* **8,** 14201–14201 CrossRef Medline
45. Gloriani, A. H., and Schütz, A. C. (2019) Humans trust central vision more than peripheral vision even in the dark. *Curr. Biol.* **29,** 1206–1210.e4 CrossRef Medline
46. Ravi, V., and Venkatesh, B. (2008) Rapidly evolving fish genomes and teleost diversity. *Curr. Opin. Genet. Dev.* **18,** 544–550 CrossRef Medline
47. Van Hooser, J. P., Liang, Y., Maeda, T., Kuksa, V., Jang, G. F., He, Y. G., Rieke, F., Fong, H. K., Detwiler, P. B., and Palczewski, K. (2002) Recovery of visual functions in a mouse model of Leber congenital amaurosis. *J. Biol. Chem.* **277,** 19173–19182 CrossRef Medline
48. Gearhart, P. M., Gearhart, C., Thompson, D. A., and Petersen-Jones, S. M. (2010) Improvement of visual performance with intravitreal administration of 9-cis-retinal in Rpe65-mutant dogs. *Arch. Ophthalmol.* **128,** 1442–1448 CrossRef Medline
49. Babino, D., Perkins, B. D., Kindermann, A., Oberhauser, V., and von Lintig, J. (2015) The role of 11-cis-retinyl esters in vertebrate cone vision. *FASEB J.* **29,** 216–226 CrossRef Medline
50. Rodriguez, K. A., and Tsin, A. T. (1989) Retinyl esters in the vertebrate neuroretina. *Am. J. Physiol.* **256,** R255–R258 CrossRef Medline
51. Radu, R. A., Hu, J., Peng, J., Bok, D., Mata, N. L., and Travis, G. H. (2008) Retinal pigment epithelium-retinal G protein receptor-opsin mediates light-dependent translocation of all-*trans*-retinyl esters for synthesis of visual chromophore in retinal pigment epithelial cells. *J. Biol. Chem.* **283,** 19730–19738 CrossRef Medline
52. Xue, Y., Shen, S. Q., Jui, J., Rupp, A. C., Byrne, L. C., Hattar, S., Flannery, J. G., Corbo, J. C., and Kefalov, V. J. (2015) CRALBP supports the mammalian retinal visual cycle and cone vision. *J. Clin. Invest.* **125,** 727–738 CrossRef Medline
53. Mata, N. L., Lichter, J. B., Vogel, R., Han, Y., Bui, T. V., and Singerman, L. J. (2013) Investigation of oral fenretinide for treatment of geographic atrophy in age-related macular degeneration. *Retina* **33,** 498–507 CrossRef Medline
54. Crowley, R., Sundaramurthi, H., UCD Biomedical Facility Staff, and Kennedy, B. (2019) University College Dublin (UCD) Zebrafish Facility Environmental Parameters. *protocols.io.* CrossRef